PNAS RESEARCH ARTICLE | NEUROSCIENCE

A noradrenergic-hypothalamic neural substrate for stress-induced sleep disturbances

Hanna Antila[a], Iris Kwak[a], Ashley Choi[a], Alexa Pisciotti[a], Ivan Covarrubias[a], Justin Baik[a], Amelia Eisch[a,b], Kevin Beier[c], Steven Thomas[d], Franz Weber[a], and Shinjae Chung[a,1]

Edited by Joseph Takahashi, The University of Texas Southwestern Medical Center, Dallas, TX; received January 12, 2022; accepted August 19, 2022

In our daily life, we are exposed to uncontrollable and stressful events that disrupt our sleep. However, the underlying neural mechanisms deteriorating the quality of non-rapid eye movement sleep (NREMs) and REM sleep are largely unknown. Here, we show in mice that acute psychosocial stress disrupts sleep by increasing brief arousals (microarousals [MAs]), reducing sleep spindles, and impairing infraslow oscillations in the spindle band of the electroencephalogram during NREMs, while reducing REMs. This poor sleep quality was reflected in an increased number of calcium transients in the activity of noradrenergic (NE) neurons in the locus coeruleus (LC) during NREMs. Opto- and chemogenetic LC-NE activation in naïve mice is sufficient to change the sleep microarchitecture similar to stress. Conversely, chemogenetically inhibiting LC-NE neurons reduced MAs during NREMs and normalized their number after stress. Specifically inhibiting LC-NE neurons projecting to the preoptic area of the hypothalamus (POA) decreased MAs and enhanced spindles and REMs after stress. Optrode recordings revealed that stimulating LC-NE fibers in the POA indeed suppressed the spiking activity of POA neurons that are activated during sleep spindles and REMs and inactivated during MAs. Our findings reveal that changes in the dynamics of the stress-regulatory LC-NE neurons during sleep negatively affect sleep quality, partially through their interaction with the POA.

sleep | stress | microarousals | sleep spindles

Significance

Good-quality sleep is essential for our well-being. Sleep disturbances can negatively affect our mental and physical health. Here, we show that acute psychosocial stress in mice disrupts sleep, by causing frequent arousals, disrupting slow (~minute) oscillations in the electroencephalogram and suppressing REMs. These changes are reflected in a frequent activation of noradrenergic neurons in the locus coeruleus (LC-NE) during NREMs. Activating LC-NE neurons disrupted sleep quality similar to stress, while inhibiting them after stress improved sleep partially through their projections to the preoptic area, a crucial sleep center. Our study reveals that LC-NE neurons and their interactions with hypothalamic sleep neurons orchestrate the sleep microarchitecture and play a crucial role in mediating the negative impact of stress on sleep.

Stress is associated with poor-quality sleep. Sleep disturbances, when untreated, have been shown to increase the risk of developing psychiatric disorders and often precede their clinical expression (1–5). Early treatment of sleep problems in turn may halt the development of psychiatric disorders. Nevertheless, little is known about the neural mechanisms responsible for stress-induced sleep disturbances.

In animal models and humans, stress disrupts various aspects of sleep (6–10). In particular, fragmented non-rapid eye movements (NREMs) due to frequent brief arousals (microarousals [MAs]) disrupts sleep continuity and may lead to cognitive impairment and anxiety (11–14). In addition, REMs abnormalities are often observed in patients with insomnia, depression, and post-traumatic stress disorder (PTSD) (15–17). In humans, psychosocial stressors are among the major sources of stress. In rodents, social stress—in particular, a conflict with an aggressive mouse—has been shown to disrupt sleep (18–26). These alterations in the sleep architecture caused by social stress may result from interactions between stress and sleep regulatory circuits. However, the identity of the involved circuits and the mechanisms by which stress regulatory neurons potentially affect the activity of the core sleep circuits are still largely unclear.

Noradrenergic (NE) neurons in the locus coeruleus (LC) have been well characterized for their role in arousal and related behaviors (27–32). In awake behaving mice, LC neurons are activated in response to salient stimuli, various stressors, novelty, or learning (33–42). A previous study found that LC neurons expressed increased levels of c-Fos during sleep following stress (43). Recently, it has been shown that during sleep, the LC plays a role in modulating the frequency of sleep spindles on an approximately minute timescale (44). This infraslow oscillation, which is also reflected in the sigma band of the electroencephalogram (EEG), is thought to gate transitions from NREMs to wakefulness or REMs (45–47), and consequently substantially influences the sleep microarchitecture. However, we still lack knowledge as to how stress-induced changes in the activity of LC-NE neurons during sleep affect the infraslow rhythm and sleep quality by interacting with sleep-regulatory neurons, in particular, in the preoptic area of the hypothalamus (POA), which is known to be crucial for sleep control (48–53). NE injection into the POA was shown to promote arousals (54), and electrical stimulation of the LC and optogenetic activation of axonal projections to the POA have been shown to modulate the activity of POA neurons (55, 56). However, it is still largely

Author contributions: H.A., F.W., and S.C. conceived the study; H.A., F.W., and S.C. designed research; H.A., F.W., and S.C. designed the methodology; J.B. and F.W. contributed software; H.A., I.K., A.C., A.P., and I.C. performed research; J.B., A.E., K.B., and S.T. contributed reagents/analytic tools; H.A., F.W., and S.C. analyzed data; H.A. created the visualization; H.A., A.E., K.B., S.T., F.W., and S.C. wrote and edited the paper; F.W. and S.C. supervised the study; and S.C. acquired the funding.

The authors declare no competing interest.

This article is a PNAS Direct Submission.

[1]To whom correspondence may be addressed. Email: shinjaec@pennmedicine.upenn.edu.

This article contains supporting information online at http://www.pnas.org/lookup/suppl/doi:10.1073/pnas.2123528119/-/DCSupplemental.

Published November 4, 2022.

unclear how the activity of POA neurons that are innervated by the LC is associated with sleep spindles and MAs during NREMs or REMs and whether interactions between the LC and POA contribute to stress-induced sleep disturbances.

In this study, using fiber photometry, we found that LC-NE neurons are rhythmically activated during NREMs in synchrony with the infraslow rhythm and that their activation is accompanied by MAs. Following acute social defeat stress, their calcium transients became more frequent, resulting in increased MAs during NREMs and suppression of REMs. In addition, opto- and chemogenetic activation of LC-NE neurons similarly disrupted sleep, and inhibiting LC-NE neurons attenuated the stress-induced MAs. Using a genetically encoded NE sensor, we found that NE is released in the POA in a brain state–dependent manner, and inhibiting LC-NE projections to the POA after stress increased REMs. Using optrode recordings, we found that stimulating LC-NE fibers in the POA suppressed the activity of REMs-active neurons. Our findings suggest a mechanism by which stress-activated LC-NE neurons projecting to the POA contribute to stress-induced sleep disturbances.

Results

The Activity of LC-NE Neurons Rhythmically Fluctuates during NREMs. To monitor the population activity of LC-NE neurons during spontaneous sleep, we injected adeno-associated viruses (AAVs) with Cre-dependent expression of the genetically encoded calcium indicator GCaMP6s into the LC of dopamine beta-hydroxylase (DBH)-Cre mice and implanted an optic fiber to measure the calcium-dependent fluorescence using fiber photometry (Fig. 1*A* and *SI Appendix*, Fig. S1*A*). Calcium imaging together with EEG and electromyography (EMG) recordings revealed that LC-NE neurons are most active during wakefulness, less active during NREMs, and nearly silent during REMs (Fig. 1 *B* and *C*; $P = 0.0005$, 0.0007, 0.0006 for NREM versus REM, NREM versus wake, and REM versus wake, respectively; detailed statistical results are shown in *SI Appendix*, Table S1), as previously described (55, 57–60). During NREMs, we found that the LC-NE activity fluctuated on an infraslow timescale of tens of seconds (Fig. 1*B*). Previous studies showed that the EEG sigma (10. 5 to 16 Hz) power displays a salient infraslow oscillation during NREMs (46, 61, 62). Consistent with these reports, the infraslow oscillation was more pronounced in the sigma than in the delta range (*SI Appendix*, Fig. S1 *B* and *C*; $P = 5.972e{-}14$). We tested whether the rhythmic fluctuations in the LC-NE activity during NREMs are correlated with this infraslow rhythm and found that the power spectral densities (PSDs) of both the ΔF/F signal and the sigma power peaked at comparable frequencies, 0.017 ± 0.005 Hz (mean ± SEM) and 0.015 ± 0.005 Hz, respectively (Fig. 1*D*). The LC-NE activity was strongly negatively correlated with the sigma power during NREMs ($P < 0.001$), and the LC-NE activity was highest at the trough of the infraslow oscillation in sigma power (Fig. 1 *E* and *F*). Compared with the delta (0.5 to 4.5 Hz) and theta (6 to 9 Hz) powers, the negative correlation was strongest for the sigma power (Fig. 1*F*; $P < 1.155e{-}12$). Thus, LC-NE neurons are periodically activated during NREMs, and the infraslow fluctuation in their activity is negatively correlated with the EEG sigma power.

In addition, we observed that MAs (wake periods ≦20 s) were often accompanied by large, regularly occurring transients in the LC-NE calcium activity (Fig. 1*B* and *SI Appendix*, Fig. S1*D*), and the calcium signal started significantly increasing 1 s before the MA onset (Fig. 1*G*; $P = 0.034$). 27.203 ± 0.029% of LC-NE calcium transients during NREMs overlapped with MAs, while during the remaining transients, NREMs was not interrupted. The ΔF/F increase was higher when it coincided with an MA (*SI Appendix*, Fig. S1*E*; $P = 1.032e{-}14$). MAs are short arousal bouts, which are characterized by a low-amplitude EEG and increased muscle tone (63–65). To test to what extent MAs differ from wakefulness and NREMs, we performed spectral analysis of the EEG and EMG signals (*SI Appendix*, Fig. S1 *F* and *G*). The delta power (0.5 to 4.5 Hz) during MAs was significantly higher than during wake episodes, but lower than during NREMs (*SI Appendix*, Fig. S1*G*; $P < 0.001$ for MA versus NREM and MA versus wake). The high-frequency gamma power (45 to 100 Hz) during MAs was significantly lower than during NREMs and wakefulness (*SI Appendix*, Fig. S1*G*; $P = 0.005$, 0.001 for MA versus NREM and MA versus wake). The EMG amplitude during MAs lay in between that during NREMs and wake (*SI Appendix*, Fig. S1*G*; $P = 0.002$, 0.023 for MA versus NREM and MA versus wake). Thus, MAs represent a unique state differing in its spectral features from NREMs and wake.

Next, we analyzed the LC-NE activity during NREMs preceding a transition to wake or REMs. We found that the LC-NE activity was lower during NREMs before a transition to REMs than to wake (*SI Appendix*, Fig. S1*H*; $P = 9.094e{-}10$), indicating that the LC-NE activity during NREMs before state transitions differs depending on whether the mouse transitions to REMs or wakefulness. Since LC neurons are activated during wake and to a lesser degree during NREMs, we wondered whether their activity gradually changes between two successive REMs episodes (inter-REM interval). We compressed each inter-REM interval to unit duration before averaging the LC-NE activity over multiple inter-REM intervals and across multiple mice. The activity was highest at the beginning of the interval and significantly decreased throughout the interval (*SI Appendix*, Fig. S1*I*; $R = -0.210$, $P = 4.697e{-}27$). When we analyzed the activity during NREMs and wake states separately throughout the inter-REM interval, the activity significantly decreased during NREMs but increased during wakefulness (*SI Appendix*, Fig. S1*J*; $R = -0.478$, 0.366, $P < 0.001$, < 0.001 for NREMs and wake). Thus, in addition to the salient modulation on the infraslow timescale, the LC activity fluctuates on the ultradian timescale in synchrony with the sleep cycle.

Acute Social Defeat Stress Leads to Frequent Activation of LC-NE Neurons during NREMs. We then investigated how acute social defeat stress affects the sleep architecture and activity of LC-NE neurons (Fig. 1*H*). We performed fiber photometry baseline recordings of these neurons. On the stress day, the experimental mouse was exposed to an aggressive CD1 mouse for physical attacks and subsequently stayed in the cage of the CD1 mouse with a perforated wall placed in between them, which prevented physical contact, but still allowed for sensory interaction. First, we examined how the acute social defeat stress changed the overall sleep architecture (*SI Appendix*, Fig. S2 *A*–*C*). The total time spent in NREMs and REMs during the 4-h recording sessions was significantly reduced due to a reduction in the frequency and duration of episodes, while the percentage of wakefulness was significantly elevated (*SI Appendix*, Fig. S2 *A*–*C*; $P < 0.001$, < 0.001, < 0.001 for percentage; $P = 0.003$, < 0.001, 0.007 for duration; $P = 0.013$, < 0.001, 0.006 for frequency of NREMs, REMs, and wake). During NREMs, the number of MAs was significantly increased, resulting in fragmented sleep with a reduced duration of NREMs bouts (Fig. 1*I* and *SI Appendix*, Fig. S2*A*; $P = 6.404e{-}5$, 0.003 for MA and duration). Furthermore, the frequency of spindles during NREMs (spindles were detected in the frontal EEG, *SI Appendix*, Fig. S2*D*), a major contributor to

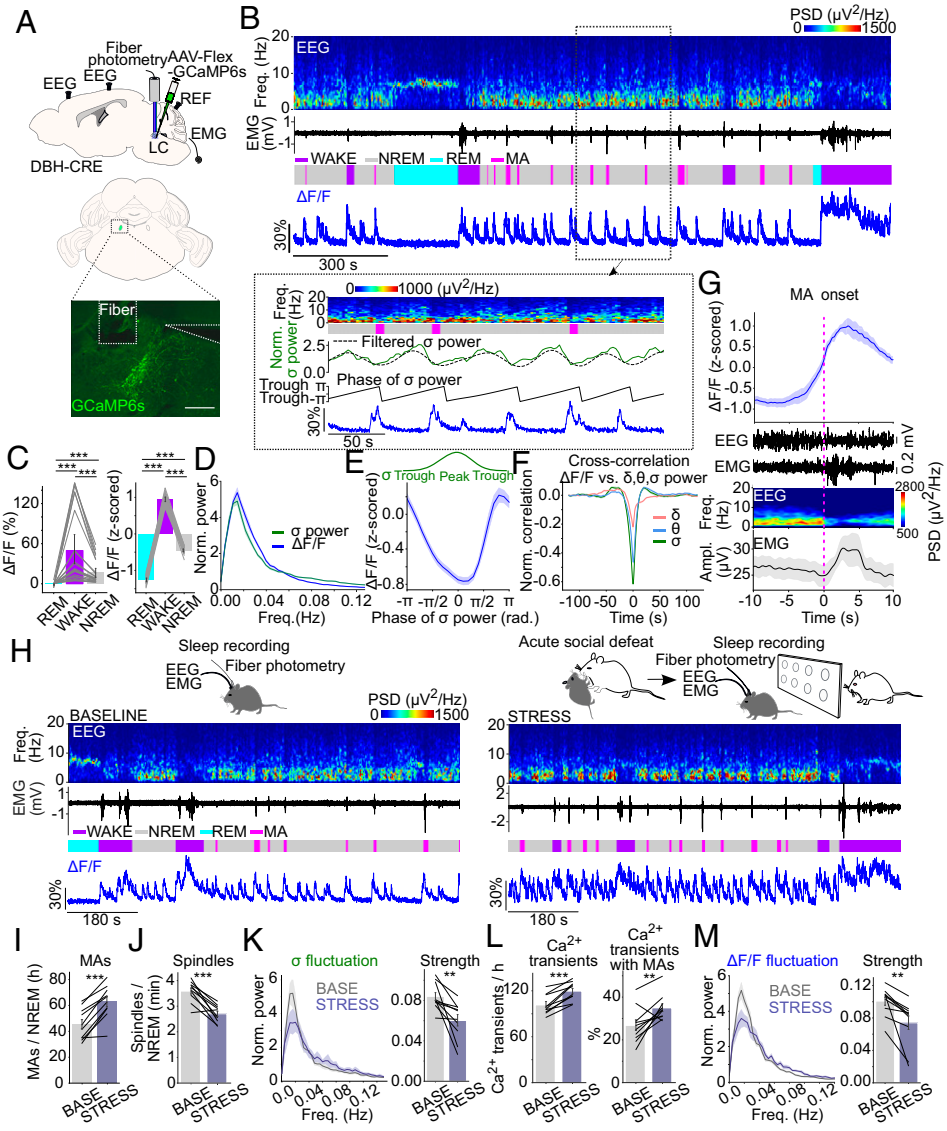

Fig. 1. LC-NE neurons are activated during spontaneous NREMs and after stress. (*A*) *Top*, Schematic of fiber photometry with simultaneous EEG and EMG recordings. Mouse brain figure adapted from the Allen Mouse Brain Atlas (© 2015 Allen Institute for Brain Science). *Bottom*, Fluorescence image of LC in a DBH-Cre mouse with AAV-FLEX-GCaMP6s injected into the LC. Scale bar, 250 μm. (*B*) *Top*, Example fiber photometry recording. Shown are parietal EEG spectrogram, EMG traces, color-coded brain states, and ΔF/F signal. *Bottom*, Parietal EEG spectrogram, brain states, EEG sigma power (10.5 to 16 Hz, green, parietal EEG), phase of EEG sigma power, and calcium signal during a selected interval (dashed box) at an expanded timescale. The filtered sigma power (dashed line) was used to determine the phase of the sigma power oscillation (middle). Freq, frequency. (*C*) Non-normalized and *Z* scored ΔF/F activity during REMs, wake, and NREMs. Bars, averages across mice; lines, individual mice; error bars, SEMs. One-way RM ANOVA followed by pairwise *t* tests with Bonferroni correction, ***$P < 0.001$. $n = 22$ mice. (*D*) Normalized PSD of sigma power in the parietal EEG and calcium activity during NREMs. The PSD for both signals was calculated only for consolidated bouts of NREMs (NREMs episodes ≧120 s, only interrupted by MAs [i.e., wake episodes ≦ 20 s]) and normalized for each animal by its mean power. Shadings, SEMs. (*E*) Average calcium activity during a single cycle of the sigma power oscillation in the parietal EEG. Each sigma power cycle was normalized in time, ranging from $-\pi$ to π rad. Shadings, SEMs. (*F*) Cross-correlation between calcium activity and parietal EEG delta, theta, or sigma power during NREMs. Shadings, SEMs. (*G*) Calcium activity changes, parietal EEG and EMG traces, EEG spectrogram, and EMG amplitude at the transition to MAs. Shadings, SEMs. (*H*) *Top*, Schematic illustrating fiber photometry for baseline sleep recordings (*Left*) and the acute social defeat paradigm (*Right*). The experimental mouse (black mouse) was first exposed to a CD1 mouse (white mouse). Afterward, a fiber photometry recording was performed in the experimental mouse while staying in the cage of the CD1 mouse, with a perforated wall placed between them. *Bottom*, Fiber photometry recordings during baseline recordings (*Left*) and after acute social defeat stress (*Right*). (*I*) Number of MAs during NREMs for the 4-h recording. (*J*) Number of sleep spindles during NREMs. Spindles were detected in the frontal EEG. (*K*) *Left*, Normalized PSD of the parietal EEG sigma power during NREMs. Shadings, 95% confidence intervals (CIs). *Right*, Strength of infraslow sigma power oscillation. (*L*) *Left*, Number of calcium transients during NREMs. *Right*, Proportion of calcium transients coinciding with MAs. The algorithm for the detection of calcium transients is described in *SI Appendix*, Fig. S1*D*. (*M*) *Left*, Normalized PSD of the calcium activity during NREMs. *Right*, Strength of the infraslow calcium activity oscillation. (*I–M*) Bars, averages across mice; lines, individual mice; error bars, SEMs. Paired *t* tests; **$P < 0.01$; ***$P < 0.001$. $n = 10$ mice (*SI Appendix*, Figs. S1 and S2 and Table S1).

the EEG sigma power (66), and the EEG sigma power were significantly decreased, while the delta power in the frontal EEG was increased after stress (Fig. 1*J* and *SI Appendix*, Fig. S2*E*, $P = 0.0003$ for spindle, $P = 0.004$, 0.007 for frontal and parietal sigma, respectively, $P = 0.046$ for frontal delta). The strength of the infraslow oscillation in the sigma power was significantly decreased (Fig. 1*K*; $P = 0.006$), suggesting that acute social defeat stress weakens the infraslow rhythm during NREMs. The stress-induced reduction in the spindle and increase of the MA frequency during NREMs may contribute to the suppression of REMs (45, 67).

Second, we examined whether stress exposure leads to changes in the LC-NE activity. During NREMs, the number of LC-NE calcium transients and the probability that they coincide with MAs was significantly enhanced after stress (Fig. 1*L* and *SI Appendix*, Fig. S1*D*; $P = 0.0001$, 0.009 for transients and probability, respectively). Consistent with the reduced strength of the sigma power oscillation, the infraslow fluctuation of the LC-NE neuron activity was reduced after stress (Fig. 1*M*; $P = 0.006$). To test whether exposure to another mouse in general influences the activity of LC neurons, we performed fiber photometry recordings, while another C57BL/6 mouse stayed on the other side of the wall in the same cage with the experimental mouse (*SI Appendix*, Fig. S2*F*). The number of MAs and spindles, the amplitude of the infraslow oscillation, the number of LC-NE neuron calcium transients, and the modulation of the ΔF/F activity were not affected (*SI Appendix*, Fig. S2 *G–K*), while the amount of NREMs was slightly increased and that of wake was decreased compared with the baseline recordings (*SI Appendix*, Fig. S2 *L–N*; $P = 0.004$, 0.002 for NREM and wake, respectively). These findings suggest that exposure to a new mouse alone does not significantly alter the LC-NE activity during sleep.

LC-NE Neurons Promote MAs and Suppress REMs. Fiber photometry recordings revealed an activation of the LC-NE neurons during MAs. To test the causal relationship between LC-NE

neuron activity and MAs, we optogenetically activated LC-NE neurons for short periods of time. DBH-Cre mice were injected with AAV-double-floxed inverted open-reading frame-channelrhodopsin-2-enhanced yellow fluorescent protein (AAV-DIO-ChR2-EYFP) into the LC (Fig. 2*A* and *SI Appendix*, Fig. S3*A*). Stimulating LC-NE neurons for 5 or 20 s (3 Hz) significantly increased the percentage of MAs during the laser interval, while decreasing NREMs and REMs (Fig. 2 *B–D*; $P = 0.001$, < 0.001 for MA, $P = 0.002$, < 0.001 for NREMs, $P = 0.004$, 0.001 for REMs, $P = 0.275$, 0.001 for wake). A 20-s stimulation also increased wakefulness, but to a lesser degree than MAs (*SI Appendix*, Fig. S3*F*; $P = 7.089e{-}7$, $20.176 \pm 1.955\%$ increase in MAs, and $6.048 \pm 1.304\%$ increase in wake). To exclude that the increase in MAs was only an effect of the short stimulation interval, we also stimulated these neurons for longer periods. A 120-s stimulation also increased the percentage of MAs at the beginning of the laser interval, but did not promote long wake episodes (Fig. 2 *C* and *D*; $P = 0.002$, 0.374 for MA and wake, respectively). Regardless of the total laser stimulation duration (5, 20, or 120 s), the distribution of the wake bout durations peaked at ~5 s (Fig. 2*F*). Furthermore, LC-NE stimulation completely suppressed REMs throughout the entire laser stimulation period (Fig. 2 *C* and *D*; $P = 0.004$, 0.001, <0.001 for 5-, 20-, and 120-s stimulation, respectively). In control mice expressing EYFP in the LC-NE neurons, laser stimulation had no significant effect on the brain state (*SI Appendix*, Figs. S3 *B–D*), and the laser-induced changes in MAs (5-, 20-, and 120-s stimulation), REMs (5, 20, and 120 s), NREMs (5 and 20 s), and wake (20 s) were significantly different between the EYFP and ChR2 groups (*SI Appendix*, Fig. S3*F*; $P < 0.001$, $P < 0.001$, $P = 0.046$ for MAs; $P = 0.02$, 0.002, 0,001 for REMs; $P = 0.001$, $P < 0.001$, $P = 0.810$ for NREMs; $P = 0.298$, 0.006, 0.265 for wake in 5-, 20-, and 120-s stimulation). Moreover, photoactivation decreased the number of spindles during the entire laser period in the ChR2 but not in the EYFP group (Fig. 2*E* and *SI Appendix*, Fig. S3*E*; $P < 0.001$ in ChR2, $P > 0.664$ in EYFP), similar to previous studies (44, 58, 59, 68). We observed that during spontaneous sleep, the number of spindles increased before MAs and sharply decreased during the MAs (Fig. 2*G*; $P = 2e{-}6$, 0.001 for before and during MAs, respectively). EEG spectral analysis revealed that stimulation in the ChR2 group for 120 s (3 Hz) significantly suppressed the sigma and theta powers and increased the delta power in the parietal and frontal EEG during NREMs, whereas EYFP control mice did not show any significant changes (*SI Appendix*, Fig. S3 *G* and *H*; $P = 0.04$, < 0.001 for delta, $P < 0.001$ for theta and sigma of parietal and frontal EEG in ChR2; $P > 0.412$ in EYFP). When tyrosine hydroxylase (TH)-Cre mice were used for optogenetic experiments, laser stimulation promoted sustained wake episodes more strongly than was observed for LC stimulation in DBH-Cre mice (*SI Appendix*, Fig. S4*I*, $P = 0.001$, < 0.001, < 0.001 for 5-, 20-, and

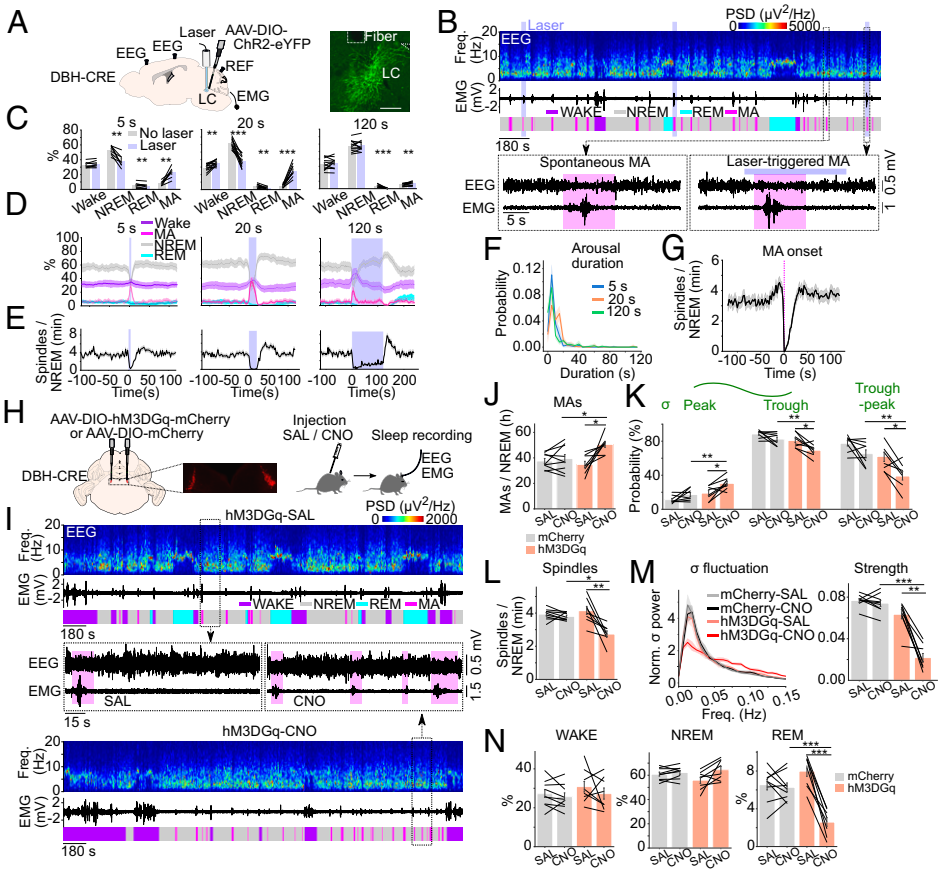

Fig. 2. LC-NE neuron activation promotes MAs and suppresses spindles and REMs. (*A*) *Left*, Schematic of optogenetic experiment. *Right*, fluorescence image of LC in a DBH-Cre mouse, with AAV-DIO-ChR2-eYFP injected into the LC. Scale bar, 200 μm. (*B*) Example trial. Shown are parietal EEG spectrogram, EMG traces, color-coded brain states, and EEG and EMG raw traces during selected periods (dashed boxes) on an expanded timescale. Blue shading, laser stimulation interval (3 Hz for 20 s). (*C*) Percentage of wake, NREMs, REMs, or MAs before and during laser stimulation (3 Hz, 5-, 20-, or 120-s stimulation). The duration of the baseline interval without laser was equal to that of the following laser interval. $n = 8$ to 12 mice. (*D*) Percentage of time spent in wake, NREMs, REMs, or MAs before, during, and after laser stimulation (blue shading), averaged from 8 to 12 mice. Shadings, 95% CIs. (*E*) Effect of laser stimulation on the number of spindles during NREMs. Spindles were detected in the frontal EEG. Shadings, 95% CIs. (*F*) Normalized histogram of the duration of episodes scored as MA (≦20 s) or wake (>20 s). Shadings, 95% CIs. The area under the curve is 1. (*G*) Number of spindles at the MA onset during spontaneous NREMs. Spindles were detected in the frontal EEG. Shadings, 95% CIs. (*H*) Schematic of chemogenetic activation experiment. *Left*, Coronal diagram of mouse brain. *Center*, Fluorescence image of LC in a DBH-Cre mouse injected with AAV-DIO-mCherry or AAV-DIO-hM3DGq-mCherry (red) into the LC. Scale bar, 500 μm. *Right*, Intraperitoneal (IP) injection of saline (SAL) or CNO (1 mg/kg) followed by EEG and EMG recordings. (*I*) Example SAL (top) and CNO (bottom) session from one hM3DGq mouse. Shown are parietal EEG spectrogram, EMG traces, color-coded brain states, and parietal EEG and EMG traces during selected periods (dashed boxes) on an expanded timescale. (*J*) Number of MAs during NREMs for the 4-h recording following SAL or CNO injection in mCherry and hM3DGq mice. $n = 8$ to 9 mice. (*K*) Probability of NREMs to MA transitions during the peak and trough of the sigma power oscillation and difference of the probability between trough and peak following SAL or CNO injection. (*L*) Number of spindles during NREMs following SAL or CNO injection. Spindles were detected in the frontal EEG. (*M*) *Left*, PSDs of the sigma power in the parietal EEG during NREMs following SAL or CNO injection. For each mouse, the spectral density was normalized by its mean power. Shadings, 95% CIs. *Right*, Strength of the sigma power oscillation. (*N*) Percentage of time in wake, NREMs, or REMs following SAL or CNO injection. (*C*, *J–N*) Bars, averages across mice; lines, individual mice; error bars, SEMs. Paired *t* tests for (*C*) and mixed ANOVA with Bonferroni correction for (*J–N*); *$P < 0.05$; **$P < 0.01$; ***$P < 0.001$ (*SI Appendix*, Figs. S3–S5 and Table S1).

120-s stimulation, respectively), which is likely attributable to the nonspecific expression of Cre-recombinase in non-NE cells in the LC and neighboring regions (69) (see Discussion). Taken together, our optogenetic activation experiments in DBH-Cre mice showed that LC-NE neuron stimulation promotes MAs regardless of the duration of laser stimulation, while strongly suppressing sleep spindles and REMs.

In a complementary experiment, we chemogenetically excited LC-NE neurons to further probe their role in the regulation of MAs. We injected AAVs encoding the excitatory designer receptors exclusively activated by designer drugs (DREADD), hM3DGq-mCherry (AAV-DIO-hM3DGq-mCherry), or mCherry (AAV-DIO-mCherry) into the LC of DBH-Cre mice (Fig. 2*H*). Immunohistochemical staining confirmed the specificity of mCherry expression (*SI Appendix*, Fig. S5*A*). Injection of the agonist clozapine-*N*-oxide (CNO) significantly increased the number of MAs during NREMs in hM3DGq mice (Fig. 2 *I* and *J*; $P = 0.034$). Previous studies reported that high doses of CNO have an effect on various sleep parameters (47, 70–72), an effect likely resulting from the back metabolism of CNO to clozapine or off-target effects, and we therefore directly compared the effect of CNO between the mCherry and hM3DGq groups. The increase in the frequency of MAs in hM3DGq mice was also significant when compared with that in mCherry mice injected with CNO (Fig. 2*J*; $P = 0.035$). MAs preferentially occur at the trough of the sigma power, where mice are more susceptible to wake up in response to external stimulation (46, 73). To quantify how strongly their occurrence is modulated by the phase of the infraslow rhythm, we calculated the proportion of MAs occurring during the trough or peak phase of the EEG sigma power. The larger the difference between these two values, the stronger the phase coupling of MAs. CNO injection reduced the phase coupling of MAs in hM3DGq mice compared with that in mCherry mice, suggesting that when LC-NE neurons are activated, the occurrence of MAs is less strongly coupled to the phase of the infraslow oscillation (Fig. 2*K*; $P = 0.005$). In addition, we found that CNO injection significantly decreased the number of spindles and the strength of the infraslow rhythm (Fig. 2 *L* and *M*; $P = 0.016$, < 0.001 for spindles and strength), which may cause the weakened phase coupling of MAs (Fig. 2*K*). Furthermore, LC-NE activation significantly suppressed REMs by decreasing the frequency of REMs episodes (Fig. 2*N* and *SI Appendix*, Fig. S5 *B* and *C*; $P < 0.001$, 0.001 for percentage and frequency). The overall time spent in wakefulness and NREMs was not significantly changed (Fig. 2*M*). EEG spectral analysis showed that similar to LC-NE optogenetic stimulation, chemogenetic stimulation significantly suppressed the sigma power and increased the delta power in the parietal and frontal EEG during NREMs (*SI Appendix*, Fig. S5*D*; $P = 0.015$, 0.009 for delta, $P = 0.046$, 0.011 for sigma in parietal and frontal EEG). Taken together, we found that both chemo- and optogenetic LC-NE activation promote MAs, while decreasing sleep spindles and suppressing transitions to REMs.

LC-NE Neuron Inhibition Reduces MAs and Increases Sleep Spindles during NREMs after Stress. To test whether inactivating LC-NE neurons reduces MAs during spontaneous sleep and alleviates stress-induced sleep disturbances, DBH-Cre mice were injected with AAVs encoding either mCherry or the inhibitory DREADD receptor hM4DGi-mCherry (AAV-DIO-mCherry or AAV-DIO-hM4DGi-mCherry). CNO was injected before baseline sleep recordings or after acute social defeat stress directly followed by sleep recordings (Fig. 3*A*). During the baseline recordings, LC-NE inhibition decreased the number of MAs (Fig. 3*C*; $P = 0.007$), resulting in an increased duration of NREMs episodes (*SI Appendix*, Fig. S6*A*; $P = 0.019$), but did not affect the proportion of MAs occurring during the peak or trough phase of the sigma power (Fig. 3*D*).

Stress significantly increased the number of MAs in mCherry mice (Fig. 3*C*; $P < 0.001$). However, LC-NE inhibition after stress exposure significantly lowered the number of MAs to levels comparable with those during spontaneous sleep (Fig. 3 *B* and *C*; mCherry-stress versus hM4DGi-stress $P = 0.008$, hM4DGi-stress versus hM4DGi-base $P = 0.185$), and consequently increased the duration of NREMs episodes (*SI Appendix*, Fig. S6*A*; mCherry-stress versus hM4DGi-stress, $P = 0.013$). Similar to the effects of chemogenetic activation, stress significantly weakened the phase coupling of MAs in mCherry mice (*SI Appendix*, Fig. S6*B*; $P = 0.002$). In contrast, in hM4DGi mice, CNO injection restored the phase coupling after stress (Fig. 3*E* and *SI Appendix*, Fig. S6*C*; mCherry-stress

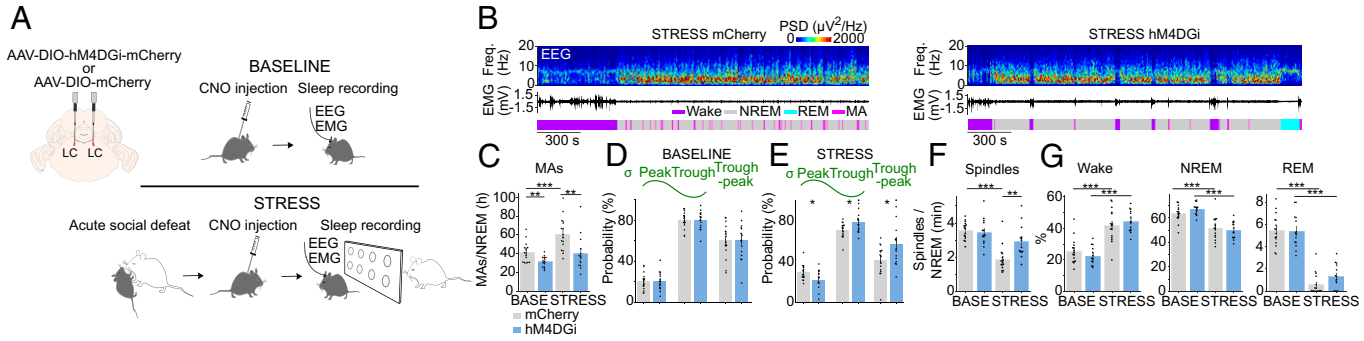

Fig. 3. Inhibiting LC-NE neurons after stress reduces MAs and increases spindles. (*A*) *Left*, Schematic depicting injection of AAV-DIO-hM4DGi-mCherry or AAV-DIO-mCherry into the LC. *Right*, Schematic of pharmacogenetic inhibition experiment combined with acute social defeat stress. For baseline, mice were injected with CNO before the sleep recording (*Top*). On the stress day, mice were exposed to acute social defeat stress and then injected with CNO. Immediately afterward, their sleep was recorded, while they were separated from the CD1 mouse by a perforated wall (*Bottom*). (*B*) Example session from mCherry (*Left*) or hM4DGi mouse (*Right*) injected with CNO after stress. Shown are parietal EEG power spectra, EMG traces, and color-coded brain states. (*C*) Number of MAs during NREMs following CNO injection (2.5 or 5 mg/kg, IP) in mCherry and hM4DGi mice during the 4-h baseline recordings and after stress. $n = 16$ mCherry and 14 hM4DGi mice. (*D*) Probability of NREMs to MA transitions during the peak and trough of the sigma power oscillation and the difference in the probability between trough and peak in baseline recordings following CNO injection. Bars, averages across mice; error bars, SEMs. (*E*) Probability of NREMs to MA transitions, depending on the phase of the sigma power oscillation in mCherry and hM4DGi mice after stress following CNO injection. Bars, averages across mice; error bars, SEMs. *t* tests; $*P < 0.05$. (*F*) Number of spindles during NREMs of baseline and stress recordings in mCherry and hM4DGi mice following CNO injection. Spindles were detected in the frontal EEG. (*G*) Percentage of time in wake, NREMs, or REMs during baseline and stress recordings in mCherry and hM4DGi mice following CNO injection. (*C*, *F*, and *G*) Bars, averages across mice; dots, individual mice; error bars, SEMs. Mixed ANOVA followed by pairwise *t* tests with Bonferroni correction; $*P < 0.05$; $**P < 0.01$; $***P < 0.001$ (*SI Appendix*, Fig. S6 and Table S1).

versus hM4DGi-stress, $P = 0.032$). Furthermore, while inhibiting LC-NE neurons did not change the number of spindles during spontaneous sleep, it significantly elevated them after stress compared with mCherry mice (Fig. 3*F*; mCherry-stress versus hM4DGi-stress $P = 0.005$). In addition, LC-NE hM4DGi mice displayed significantly higher EEG sigma power compared with mCherry mice after stress (*SI Appendix*, Fig. S6*D*; $P < 0.001$ in parietal and frontal EEGs). Inhibiting LC-NE neurons during baseline and after stress suppressed the strength of the infraslow fluctuation and shifted the peak to a lower frequency corresponding to a slower infraslow oscillation, which in turn may result in fewer MAs (*SI Appendix*, Fig. S6*E*; $P = 1.942e{-}5$, 0.037 for strength, $P = 0.0002$, 0.004 for peak frequencies).

The overall amount of time spent in wake, NREMs, and REMs during spontaneous sleep and sleep after stress exposure was not altered by LC-NE inhibition (Fig. 3*G*). Thus, while LC-NE activity does not control the overall time spent in each brain state, it plays an important role in regulating the frequency and timing of MAs as well as sleep spindles during NREMs after stress exposure and thereby affects the overall sleep quality.

NE Release in the POA Promotes MAs While Suppressing REMs. Previous in vitro studies showed that putative sleep cells in the POA characterized by the presence of low threshold spikes are inhibited by NE application (74, 75). However, it is unknown whether NE is released in the POA during sleep in vivo. To examine NE release in the POA, we expressed the genetically encoded sensor $GRAB_{NE}$ (76) in POA neurons and implanted an optic fiber for fiber photometry (Fig. 4*A* and *SI Appendix*, Fig. S7*A*). The NE levels were highest during wake, lower during NREMs, and lowest during REMs (Fig. 4 *B* and *C*; $P = 0.0001$, 0.0005, 0.0001 for NREM versus REM, NREM versus wake, and REM versus wake). During NREMs, the NE levels were negatively correlated with the sigma power (Fig. 4 *B*, *D*, and *E*; $P < 0.001$), similar to the activity of LC-NE neurons (Fig. 1*F*).

Next, we tested how activation of the LC-NE projections to the POA ($NE^{LC\rightarrow POA}$) affects the brain state (Fig. 4*F*). We injected AAVs expressing ChR2-EYFP into the LC of DBH-Cre mice and implanted an optic fiber into the POA (*SI Appendix*, Fig. S7*B*). Optogenetic activation of the LC-NE fibers in the POA (3 Hz for 20 s, 5 Hz for 20 s, and 5 Hz for 120 s) increased the percentage of MAs, while decreasing REMs and NREMs (Fig. 4 *G–I*; $P = 0.002$, < 0.001, 0.019 for MA, $P = 0.006$, 0.016, 0.001 for REMs, $P = 0.002$, 0.002, 0.127 for NREMs after 3 Hz for 20 s, 5 Hz for 20 s, and 5 Hz for 120 s stimulation). The number of spindles was significantly decreased by laser stimulation (Fig. 4*J*; $P < 0.001$, < 0.001, 0.018). In EYFP control mice, laser stimulation had no significant effect on the brain state and spindles (*SI Appendix*, Fig. S7 *D–G*). In addition, we chemogenetically activated the $NE^{LC\rightarrow POA}$ neurons by injecting AAVs with high retrograde efficiency encoding hM3DGq-mCherry (AAV-retro-DIO-hM3DGq-mCherry) or mCherry (AAV-retro-DIO-mCherry) into the POA of DBH-Cre mice (Fig. 4*K*). Following CNO injection, the frequency of MAs was significantly increased, while the phase coupling of MAs and the number of spindles were decreased in retro-hM3DGq mice compared with that in retro-mCherry mice similar to the effects found with the chemogenetic activation of LC neurons (Fig. 4 *L–O*; $P = 0.027$, < 0.001, < 0.001 for MAs, coupling, and spindles, respectively). CNO reduced the strength of the infraslow rhythm only within the retro-hM3DGq group, but not when compared with the mCherry group injected with CNO (*SI Appendix*, Fig. S7*H*; hM3DGq-SAL versus hM3DGq-CNO, $P = 0.005$) suggesting that the projection of LC-NE neurons to the POA plays only a minor role in this process. In addition, CNO injection significantly suppressed REMs without affecting the amount of wakefulness and NREMs in retro-hM3DGq mice compared with that in retro-mCherry mice (Fig. 4*P*; mCherry-CNO versus hM3DGq-CNO $P = 1.000$, 1.000, < 0.001, hM3DGq-SAL versus hM3DGq-CNO $P = 0.115$, 0.044, < 0.001 for wake, NREMs, and REMs, respectively). The duration of NREMs episodes was decreased, while their frequency was elevated (*SI Appendix*, Fig. S7*I*; $P = 0.018$, 0.003 for duration and frequency, respectively). The reduction in REMs was caused by a reduced frequency in REMs episodes (*SI Appendix*, Fig. S7*I*; $P < 0.001$). Thus, $NE^{LC\rightarrow POA}$ projections alter the sleep quality by preventing transitions to REMs, suppressing sleep spindles, and fragmenting NREMs through an increased number of MAs.

To identify the presynaptic inputs specifically regulating the activity of the $NE^{LC\rightarrow POA}$ neurons, we mapped their monosynaptic inputs by cell-type-specific tracing the relationship between input and output (*SI Appendix*, Fig. S8*A*) (77, 78). We found green fluorescent protein–labeled presynaptic neurons in multiple brain regions (*SI Appendix*, Fig. S8*B*). Interestingly, 30.8 ± 5.0% of inputs came from the medulla, whereas other brain regions known to innervate LC-NE neurons, such as the amygdala and hypothalamus, provided relatively minor inputs (7.2 ± 1.0% and 17.5 ± 2.0%). Inhibition of the REMs-suppressing $NE^{LC\rightarrow POA}$ neurons by presynaptic medulla neurons may contribute to the REMs-promoting effect observed for the activation of ventral medulla GABAergic neurons (79).

Inhibiting LC-NE Neurons Projecting to the POA after Stress Decreases MAs and Increases REMs and Sleep Spindles. To test whether inhibiting the LC-NE neurons projecting to the POA ($NE^{LC\rightarrow POA}$) alleviates stress-induced sleep disturbances, we chemogenetically inhibited them during spontaneous sleep and after acute social defeat stress (Fig. 5*A*). AAV-retro-DIO-mCherry or AAV-retro-DIO-hM4DGi-mCherry was injected into the POA of DBH-Cre mice. The number of MAs and their dependence on the phase of the sigma power was not altered by $NE^{LC\rightarrow POA}$ inhibition during baseline sleep (Fig. 5 *C* and *D*). Stress significantly increased the number of MAs (Fig. 5*C*; $P = 0.024$) and shortened NREMs bouts in mCherry mice (*SI Appendix*, Fig. S6*F*; $P = 0.01$). $NE^{LC\rightarrow POA}$ inhibition after stress led to a significant decrease in the number of MAs (Fig. 5 *B* and *C*; retro-mCherry-stress versus retro-hM4DGi-stress $P = 0.048$). $NE^{LC\rightarrow POA}$ inhibition after stress significantly strengthened the coupling of MAs to the infraslow rhythm (Fig. 5*E*; $P < 0.001$). During NREMs after stress, the number of spindles was decreased in mCherry mice, and this decrease was reversed by $NE^{LC\rightarrow POA}$ inhibition to levels comparable with spontaneous sleep (Fig. 5*F*; retro-mCherry-base versus retro-mCherry-stress $P = 0.049$, retro-mCherry-stress versus retro-hM4DGi-stress $P = 0.048$, retro-hM4DGi-base versus retro-hM4DGi-stress $P = 1.000$). $NE^{LC\rightarrow POA}$ inhibition during baseline and after stress did not affect the strength of the infraslow fluctuations in the sigma power (*SI Appendix*, Fig. S6*G*). $NE^{LC\rightarrow POA}$ inhibition significantly increased REMs after stress when compared with the mCherry group (Fig. 5*G*; retro-mCherry-stress versus retro-hM4DGi-stress $P = 0.013$). Together, these findings suggest that the activity of $NE^{LC\rightarrow POA}$ contributes to the stress-induced changes in REMs, MAs, and sleep spindles following stress.

LC-NE Projections Regulate REMs-Active Cells in the POA. Previous studies revealed the existence of neurons in the POA that are most strongly activated during REMs (R-max), in addition

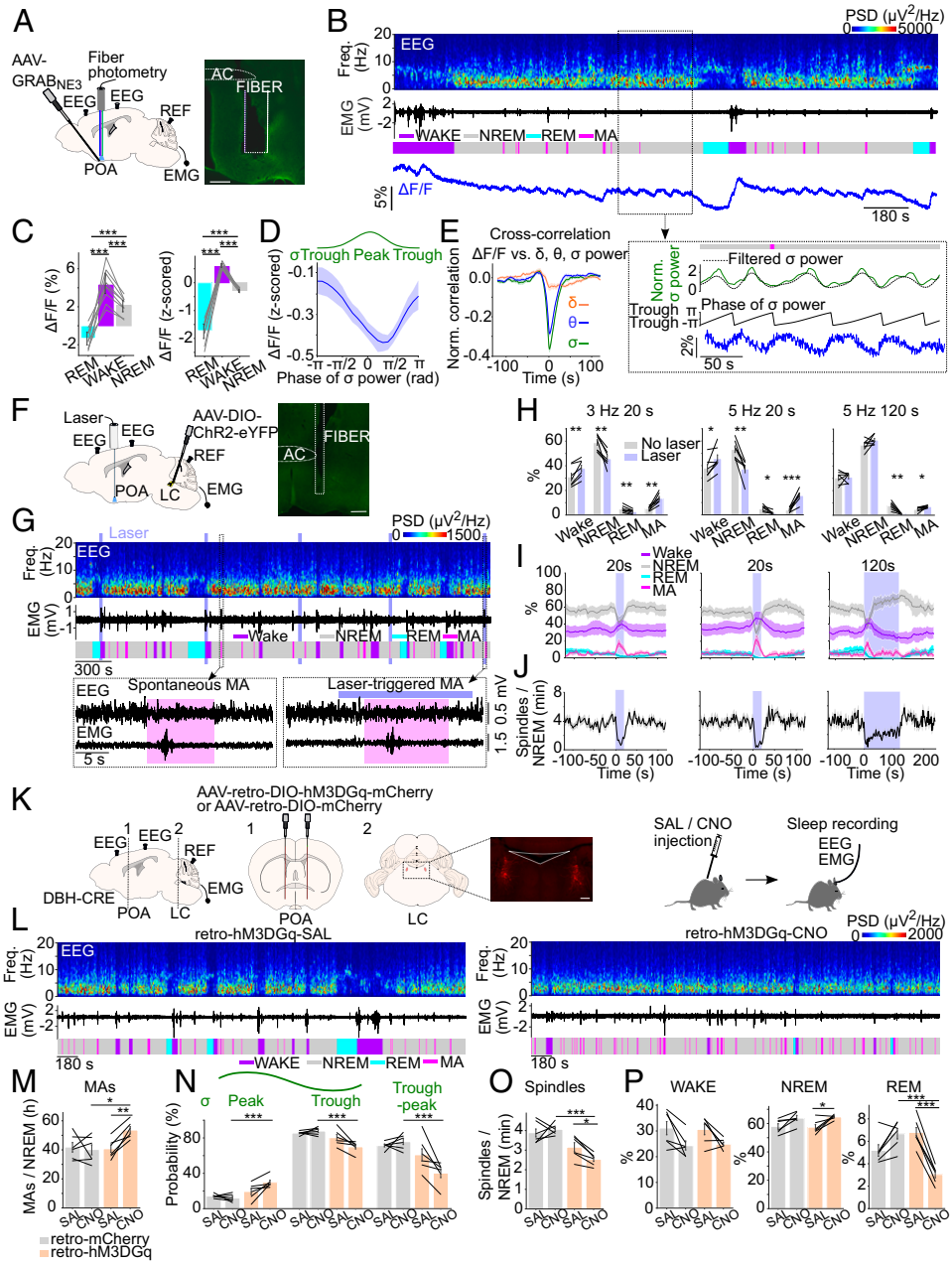

Fig. 4. $NE^{LC\rightarrow POA}$ activation promotes MAs and suppresses spindles and REMs. (*A*) *Left*, Schematic of fiber photometry recordings to monitor NE levels in the POA using the $GRAB_{NE}$ sensor. *Right*, Fluorescence image of POA in a mouse injected with AAV-$GRAB_{NE3}$ into the POA. Scale bar, 250 μm. (*B*) *Top*, Example fiber photometry recording. Shown are parietal EEG spectrogram, EMG traces, color-coded brain states, and ΔF/F signal. *Bottom*, Brain states, EEG sigma power (10.5 to 16 Hz, green, parietal EEG), phase of EEG sigma power, and calcium signal during a selected interval (dashed box) at an expanded timescale. The filtered sigma power (dashed line) was used to determine the phase of the sigma power oscillation (middle). (*C*) Non-normalized and *Z* scored ΔF/F activity during REMs, wake, and NREMs. Bars, averages across mice; lines, individual mice; error bars, SEMs. One-way RM ANOVA followed by pairwise *t* tests with Bonferroni correction; ***$P <$ 0.001. n = 9 mice. (*D*) Average calcium activity during a single cycle of the sigma power oscillation. Each sigma power cycle was normalized in time, ranging from $-\pi$ to π rad. Shadings, SEMs. (*E*) Cross-correlation between calcium activity and parietal EEG delta, theta, or sigma power during NREMs. Shadings, SEMs. (*F*) *Left*, Schematic of optogenetic experiment for stimulating axonal projections of LC-NE neurons in the POA. *Right*, Fluorescence image of POA in a DBH-Cre mouse injected with AAV-DIO-ChR2-eYFP into the LC and an optic fiber implanted into the POA. Scale bar, 200 μm. (*G*) Example trial. Shown are parietal EEG spectrogram, EMG traces, color-coded brain states, and EEG and EMG traces during selected periods (dashed boxes) on an expanded timescale. Blue shading, laser stimulation interval (3 Hz for 20 s). (*H*) Percentage of wake, NREMs, REMs, or MAs before and during laser stimulation (3 Hz for 20-s, 5 Hz for 20-s, or 5 Hz for 120-s stimulation). n = 7 mice. (*I*) Percentage of wake, NREMs, REMs, or MAs before, during, and after laser stimulation (blue shading), averaged across 7 mice. Shadings, 95% CIs. (*J*) Effect of laser stimulation on the number of spindles during NREMs. Shadings, 95% CIs. Spindles were detected in the frontal EEG. (*K*) Schematic of pharmacogenetic activation experiment to target NE neurons projecting to the POA. *Left*, Sagittal and coronal diagrams of mouse brain, fluorescence image of LC in a DBH-Cre mouse injected with AAV-retro-DIO-mCherry or AAV-retro-DIO-hM3DGq-mCherry (red) into the POA. 80.5 ± 2.5% of mCherry cells were found in the LC (186/233 cells, n = 3 mice). Scale bar, 250 μm. *Right*, Schematic depicting sleep recording following SAL or CNO (1 mg/kg) injection. (*L*) Example SAL (*Left*) and CNO (*Right*) session from one retro-hM3DGq mouse. (*M*) Number of MAs during NREMs for the 4-h recording following SAL or CNO injection in retro-mCherry and retro-hM3DGq mice. n = 6 mice. (*N*) Probability of NREMs to MA transitions during the peak and trough of the sigma power oscillation, and the difference in the probability between trough and peak following SAL or CNO injection. (*O*) Number of spindles during NREMs following SAL or CNO injection. Spindles were detected in the frontal EEG. (*P*) Percentage of time in wake, NREMs, or REMs following SAL or CNO injection. (*H*, *M–P*) Bars, averages across mice; lines, individual mice; error bars, SEMs. Paired *t* tests for (*H*) and mixed ANOVA with Bonferroni correction for (*M-P*); *$P <$ 0.05; **$P <$ 0.01; ***$P <$ 0.001 (*SI Appendix*, Figs. S7 and S8 and Table S1).

to NREMs- and wake-active neurons (48, 52, 80). To specifically test whether the R-max neurons are inhibited by the NE projections to the POA and whether their activity changes during sleep, we performed optrode recordings in the POA. AAV-DIO-ChR2 was injected into the LC of DBH-Cre mice and an optrode was implanted into the POA to determine the brain state–dependent activity of POA neurons and to probe whether their spiking was significantly modulated by $NE^{LC\rightarrow POA}$ fiber stimulation (Fig. 6*A*). Laser pulse trains (5- or 10-Hz pulses, 5 s per train) were applied every 3 to 5 min to identify single units exhibiting significant laser-evoked increases or decreases in their activity during the laser interval.

We recorded a total of 137 single units from 16 mice: 43.8% were most active during REMs (R-max), 12.4% showed highest activity during NREMs (NR-max), and 24.1% fired most during wake (W-max); 19.7% of the cells were not modulated by the brain state (*SI Appendix*, Fig. S9 *A–E*; 60, 17, 33, and 27 cells/137 total cells, respectively). We further divided R-max cells into neurons that were more active during NREMs than wake (R-NR) or vice versa (R-W) (*SI Appendix*, Fig. S9 *B* and *C*). We then investigated whether these different types of POA neurons are differentially modulated by $NE^{LC\rightarrow POA}$ fiber stimulation.

Optogenetic stimulation of $NE^{LC\rightarrow POA}$ fibers significantly decreased the firing rates during the laser interval in 32.8% of

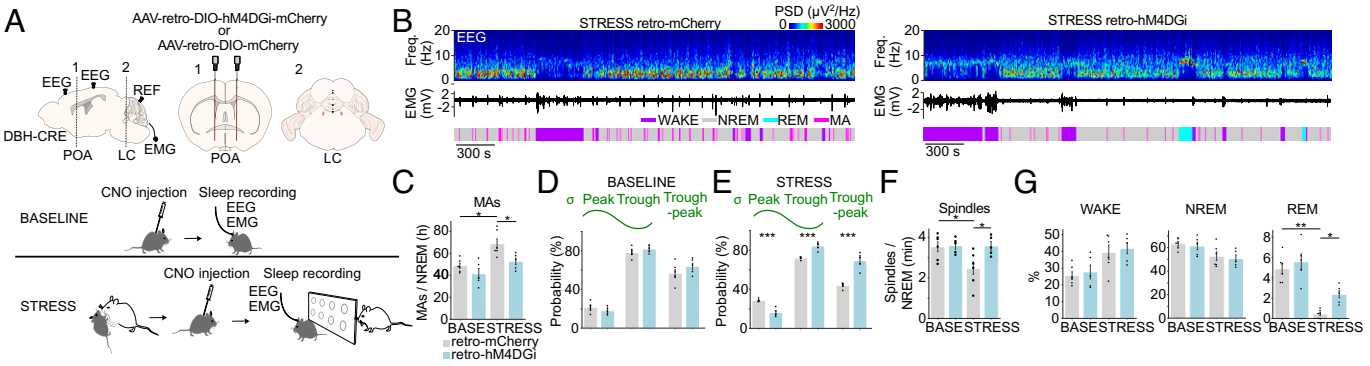

Fig. 5. Inhibiting $NE^{LC \rightarrow POA}$ neurons decreases MAs and increases REMs and sleep spindles after stress. (*A*) *Top*, Schematic depicting injection of AAV-retro-DIO-hM4DGi-mCherry or AAV-retro-DIO-mCherry into the LC. *Bottom*, Schematic of pharmacogenetic inhibition experiment combined with acute social defeat stress. (*B*) Example session from retro-mCherry (*Left*) or retro-hM4DGi (*Right*) expressing mouse injected with CNO after stress. Shown are parietal EEG power spectra, EMG traces, and color-coded brain states. (*C*) Number of MAs during NREMs following CNO injection (2.5 mg/kg, IP) in retro-mCherry and retro-hM4DGi mice during the 4-h baseline recordings and after stress. $n = 6$ retro-mCherry and 5 retro-hM4DGi mice. (*D*) Probability of NREMs to MA transitions during the peak and trough of the sigma power oscillation and the difference in the probability between trough and peak in baseline recordings of retro-mCherry and retro-hM4DGi mice following CNO injections. Bars, averages across mice; error bars, SEMs. (*E*) Probability of NREMs to MA transitions depending on the phase of the sigma power oscillation in retro-mCherry and retro-hM4DGi mice after stress following CNO injections. Bars, averages across mice; error bars, SEMs. *t* test; ***$P < 0.001$. (*F*) Number of spindles during NREMs of baseline and stress recordings in retro-mCherry and retro-hM4DGi mice following CNO injection. Spindles were detected in the frontal EEG. (*G*) Percentage of time in wake, NREMs, or REMs during baseline and stress recordings in retro-mCherry and retro-hM4DGi mice following CNO injection. (*C*, *F*, and *G*) Bars, averages across mice; dots, individual mice; error bars, SEMs. Mixed ANOVA followed by pairwise *t* tests with Bonferroni correction; *$P < 0.05$; **$P < 0.01$ (*SI Appendix*, Fig. S6 and Table S1).

the recorded POA neurons and excited the activity in 12.4% of neurons (Fig. 6 *B* and *C* and *SI Appendix*, Fig. S9 *F* and *G*; 45 and 17/137 cells). The firing rates of the inhibited POA population were on average highest during REMs, followed by NREMs and wake (Fig. 6 *D*–*F*; $P = 0.019$, 0.0001, 0.0008 for REM versus NREM, REM versus wake. and NREM versus wake, respectively). Individually, 23 units were classified as R-max neurons, 11 units as NR-max, and 5 units as W-max neurons (Fig. 6 *G* and *H* and *SI Appendix*, Fig. S9 *H* and *I*). Among the 23 R-max cells, the majority (20 cells) were R-NR cells whose firing rates were positively correlated with the EEG theta and sigma powers during NREMs (Fig. 6 *F* and *G*; $P =$ 2.360e−13, 1.318e−12 for theta and sigma, respectively). In addition, we found that their firing rates were significantly increased during sleep spindles (detected from the parietal EEG, *SI Appendix*, Fig. S9*L*) and decreased during MAs (Fig. 6*G*; $P = 0.000001$, < 0.001 for spindles and MAs, respectively). Interestingly, NR-max cells were only part of the inhibited POA population and their firing rates were positively correlated with the delta, theta, and sigma power (Fig. 6*H*; $P =$ 0.0005, 0.0005, 0.0004 for delta, theta, and sigma, respectively). Their activity was not significantly modulated by sleep spindles, but decreased during MAs (Fig. 6*H*; $P = 0.417$, 0.0002 for spindles and MAs, respectively).

The average activity of the population of excited units was higher during REMs and wake than during NREMs (Fig. 6 *I*–*K*; $P = 0.0008$, 0.611, 0.0003, for REM versus NREM, REM versus wake, and NREM versus wake, respectively). Individually, 8 cells were W-max, 6 cells were R-max, and the remaining 3 cells were not significantly modulated by the brain state (Fig. 6 *L* and *M* and *SI Appendix*, Fig. S9 *J* and *K*). All of the R-max cells were classified as R-W cells. The firing rates of the excited W-max cells were negatively correlated with the theta and sigma powers during NREMs (Fig. 6 *K* and *L*; $P =$ 0.003, 0.0001 for theta and sigma, respectively). In contrast to NR-max and R-NR units, the activity of W-max and R-W cells was not significantly modulated by sleep spindles (Fig. 6 *L* and *M*), but significantly increased during MAs ($P = 0.003$, 0.046 for W-max and R-W cells, respectively). Thus, among R-max cells, R-NR and R-W cells form two distinct subgroups based on their activity profile during NREMs. R-NR neurons were largely overrepresented in the POA population inhibited by $NE^{LC \rightarrow POA}$ fiber stimulation, and their inhibition may lead to the suppression of REMs after stress. In contrast, excitation of the R-W and W-max units by the LC may contribute to the stress-induced increase in MAs.

Discussion

Combining opto- and chemogenetic manipulation, in vivo calcium imaging, and electrophysiology with an acute social defeat stress paradigm in mice, we have identified a pathway for stress-induced sleep disturbances. We found that the calcium activity of LC-NE neurons rhythmically fluctuates during NREMs, and an increase in their activity during NREMs often preceded MAs (Fig. 1). Acute social defeat stress reduced the overall amount of sleep and deteriorated its quality characterized by frequent MAs during NREMs, which were reflected in an increased number of LC-NE calcium transients during NREMs (Fig. 1). Chemo- and optogenetic stimulation of LC-NE neurons similarly caused an increase in MAs during NREMs and suppressed REMs and sleep spindles (Fig. 2). Inhibiting LC-NE neurons attenuated the stress-induced increase in MAs and reduction of spindles (Fig. 3). Using a genetically encoded NE sensor, we showed that NE is released in the POA during sleep (Fig. 4). Inactivating the axonal projections of the LC-NE neurons to the POA after stress decreased MAs and increased the amount of REMs and the frequency of spindles (Fig. 5). Optrode recordings demonstrated that LC-NE neurons projecting to the POA inhibit R-NR-active neurons (Fig. 6). Our results suggest that stress-induced sleep disturbances are partially mediated by the LC-NE projection to the POA.

LC-NE Activity during Sleep after Acute Social Defeat Stress. The role of LC-NE neurons in regulating wake-related behaviors has been extensively investigated [reviewed by Poe et al. (30)]. Previous studies as well as ours have demonstrated that LC-NE neurons are most active during wakefulness, but are also activated during sleep (40, 55, 57–59, 81). The activity of LC-NE neurons during sleep has been shown to be important for sensory evoked awakenings, regulation of sleep spindles,

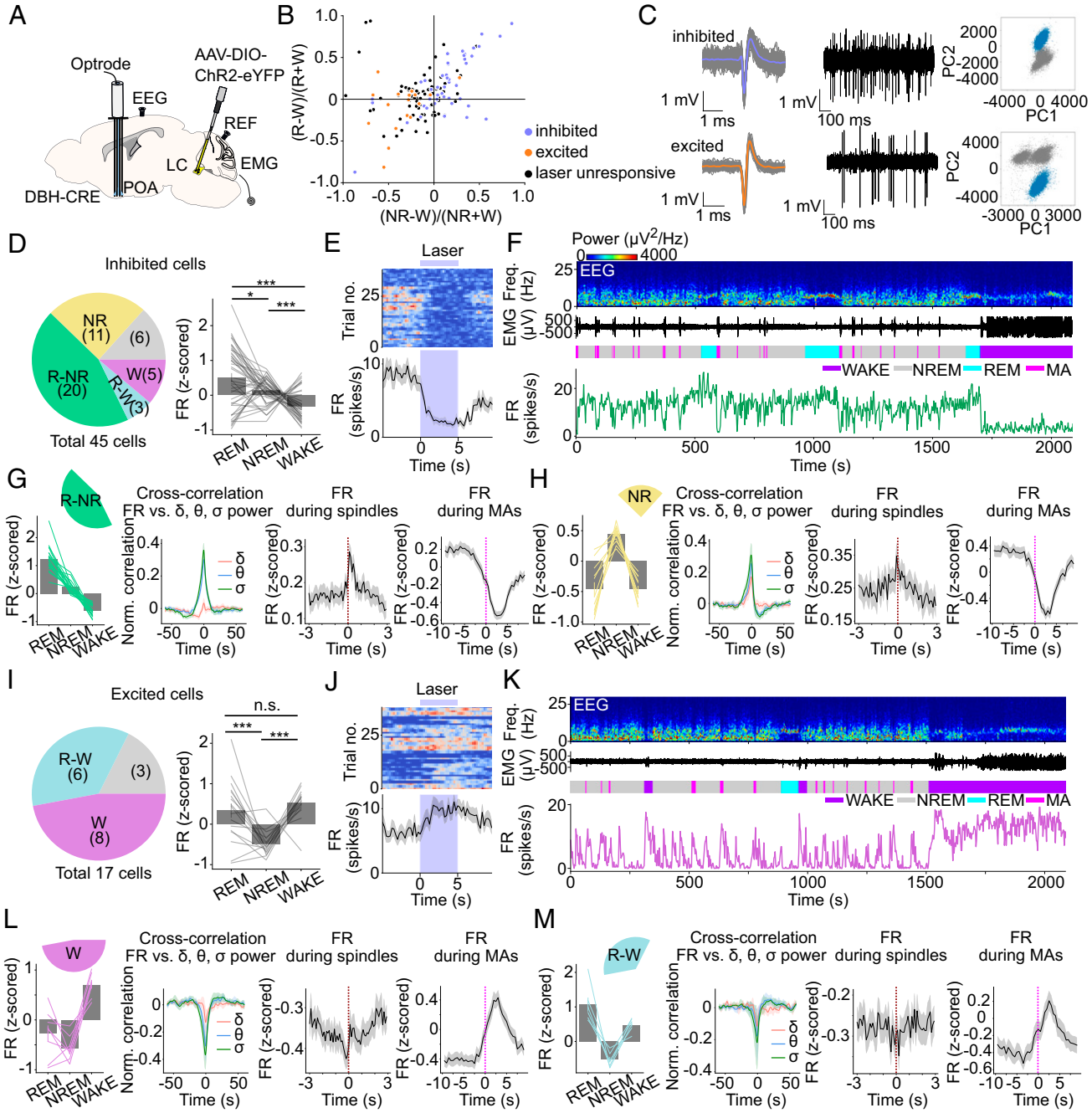

Fig. 6. Impact of $NE^{LC\rightarrow POA}$ axonal stimulation in the activity of POA neurons. (*A*) Schematic of optrode recordings to examine activity changes of POA neurons upon $NE^{LC\rightarrow POA}$ axonal stimulation. AAV-DIO-ChR2-eYFP was injected into the LC of a DBH-Cre mouse and an optrode was implanted into the POA, to record single POA units while stimulating LC-NE fibers. (*B*) Firing rate modulation of 45 inhibited (blue), 17 excited (orange), and 75 laser unresponsive (black) units. W, wake; R, REM; NR, NREM. (*C*) *Left* and *Center*, Spontaneous spike waveforms of example units that were inhibited (*Top*) or excited (*Bottom*) by $NE^{LC\rightarrow POA}$ laser stimulation. *Right*, Principal components (PC1 and PC2) of the spike waveforms. (*D*) Firing rates of 45 inhibited neurons during different brain states. *Left*, Pie chart showing the distribution of different subtypes within the inhibited units. Based on their brain state–dependent activity, units were subdivided into NR-max (NR), W-max (W), R-NR, R-W cells, and units not modulated by the brain state. *Right*, Average activity of inhibited units during REMs, NREMs, and wake; gray bars, averages across units; lines, individual units; error bars, SEMs. (*E*) *Top*, Spike raster showing multiple laser stimulation trials (10 Hz, 10 ms, 5 s). *Bottom*, Firing rates before, during, and after laser stimulation. Shadings, SEMs. (*F*) Firing rates of an example unit suppressed by $NE^{LC\rightarrow POA}$ laser stimulation. Shown are parietal EEG spectrogram, EMG traces, and color-coded brain states and the firing rates. (*G*) R-NR neurons that were significantly inhibited by $NE^{LC\rightarrow POA}$ stimulation. *Left*, Firing rates during different brain states. Gray bars, averages across units; lines, individual units; error bars, SEMs. *Center Left*, Cross-correlation between firing rates and parietal EEG delta, theta, or sigma power during NREMs. Shadings, 95% CIs. *Center Right*, Average firing rate during sleep spindles. 0 s corresponds to the sleep spindle onset. Spindles were detected in the parietal EEG. Shadings, SEMs. *Right*, Average firing rate during MAs. 0 s corresponds to the MA onset. Shadings, ±SEMs. (*H*) NR-max neurons that were significantly inhibited by $NE^{LC\rightarrow POA}$ stimulations. (*I*) Firing rates of 17 excited neurons during different brain states. *Left*, Pie chart showing the distribution of different subtypes within the excited units. *Right*, Average activity of excited units during REMs, NREMs, and wake. (*J*) *Top*, Spike raster showing multiple laser stimulation trials (10 Hz, 10 ms, 5 s). *Bottom*, Firing rates before, during, and after laser stimulation. (*K*) Firing rates of an example unit excited by $NE^{LC\rightarrow POA}$ laser stimulation. (*L*) W-max neurons that were significantly excited by $NE^{LC\rightarrow POA}$ stimulations. (*M*) R-W neurons that were significantly excited by $NE^{LC\rightarrow POA}$ stimulations. (*D* and *I*) Wilcoxon signed rank test with Bonferroni correction; **P* < 0.05; ****P* < 0.001 (*SI Appendix*, Fig. S9 and Table S1).

and cortical up/down states (36, 44, 57–59, 81, 82). Our findings corroborate that LC neurons are activated during NREMs, and, importantly, demonstrate that stressful experiences involving social conflict influence the subsequent activity of LC neurons during sleep. Similar to the REMs-suppressing GABAergic neurons in the ventrolateral periaqueductal gray (83), the LC activity is lower before transitions to REMs than to wakefulness, and therefore the heightened number of LC calcium transients after stress exposure may prevent the neural activity to drop sufficiently low to allow for transitions to REMs. The elevated number of peaks in the LC activity during sleep led to an increased frequency of MAs, which in turn likely affects overall sleep quality. MAs occur in rodents and humans during sleep, and their frequency is inversely correlated with sleep depth (63–65, 73, 84–86) and the propensity to enter REMs (67).

Activation of LC-NE Neurons Promotes MAs. Opto- and chemogenetic stimulation of LC-NE neurons induced MAs, while having little effect on promoting long wake episodes (Fig. 2). Behavioral and electrophysiological analysis suggests that MAs are distinct from sustained wake periods; their EEG high-frequency gamma power is reduced compared to wake, and cortical neurons show a different firing pattern during MAs (64, 65). This suggests that the circuits underlying sustained wake and MAs may differ from one another. Our finding that LC activation reliably triggers MAs indicates that the LC may be an integral part of the network regulating the induction and frequency of MAs during sleep. Previous studies showed that opto- or chemogenetic stimulation of the LC triggered immediate arousals from sleep (58, 68) and promoted wakefulness (55, 87–89). The strong wake-promoting effect of LC stimulation in these latter studies may be attributed to the usage of TH-Cre mice. Ectopic transgene expression driven by the TH promoter have been previously described in TH-Cre mice (90–93). A recent study systematically compared TH-Cre and DBH-Cre mice for transgene expression in the LC and nearby regions and found nonspecific labeling of non-noradrenergic neurons in TH-Cre mice (69), and TH-expressing cells in the dorsal raphe and parabrachial nucleus adjacent to the LC have been shown to be strongly wake promoting (94–96) (*SI Appendix*, Fig. S4*A*).

Our findings show that chemogenetic LC inhibition decreased MAs and thereby increased the duration of NREMs episodes without changing the overall time spent in sleep and wakefulness. Studies lesioning the LC or genetically ablating DBH in the brain found either no changes in the overall sleep architecture (97–100) or an increase in NREMs (101–103) [reviewed by Ouyang et al. (103)]. Opto- and chemogenetic inhibition of the LC using TH-Cre mice and knockdown of DBH in the LC led to an increase in NREMs during the dark phase (55, 87, 104). The number of MAs is higher during the dark phase (73), and it remains to be investigated whether LC neurons differentially regulate MAs and wakefulness depending on the circadian phase. Simultaneous lesion of cholinergic, histaminergic, and noradrenergic neurons did not change the total amount of wakefulness, but did result in more consolidated NREMs bouts, suggesting that these neuromodulatory neurons play an important role in regulating the sleep microarchitecture, but not the overall amount of sleep (97).

Inhibiting LC-NE neurons after stress exposure effectively attenuated the stress-induced MA increase. Our data suggest that changes in the LC activity during sleep underlie decreased sleep quality after stressful experiences. The neural mechanisms by which stressful events lead to more frequent calcium transients of LC neurons during sleep remain to be elucidated. Acute social stress in rats has been shown to shift the LC activity toward a high tonic state characterized by an increased spontaneous discharge rate (42). We speculate that similar mechanisms underlie the observed changes in the LC activity and MAs during sleep following stress exposure.

The Role of LC-NE Innervation to the POA. Our results demonstrate an important role of the NE projections to the POA in regulating REMs, likely through the suppression of R-NR-active neurons in the POA. c-Fos immunohistochemistry and lesion studies suggested an important role of the POA in REMs control and homeostasis (49, 105, 106). In addition, POA GABAergic neurons projecting to the tuberomammillary nucleus (TMN) are REMs-active and REMs-promoting, and their activity during NREMs is positively correlated with the EEG theta and sigma powers (48), similar to the properties of the R-NR-active cells that were inhibited by $NE^{LC\rightarrow POA}$ fiber stimulation (Fig. 6).

$NE^{LC\rightarrow POA}$ fiber stimulation activates neurons that are active during wakefulness or both wakefulness and REMs. Glutamatergic neurons in the POA have been shown to be activated after stress (107), and optogenetically activating POA glutamatergic neurons projecting to the TMN strongly promotes wakefulness (48). We therefore speculate that POA neurons excited by $NE^{LC\rightarrow POA}$ fiber stimulation are glutamatergic. In an animal model of stress-induced insomnia, both sleep-promoting areas such as the POA and wake-regulatory regions, including the TMN and LC, have been found to be simultaneously activated based on c-Fos immunohistochemistry (43). However, the specific cell types of the c-Fos-labeled POA neurons are unknown, which makes it difficult to determine whether sleep- or wake-active neurons became activated given that they are intermingled within this region (48). Uncovering the genetic identity of POA neurons that are either excited or inhibited by $NE^{LC\rightarrow POA}$ fiber stimulation or stress will greatly facilitate selective targeting of these neurons for further circuit analysis and elucidate how various aspects of sleep are affected by stress.

Infraslow Oscillation of LC Activity and Sleep Fragility after Stress. In mice, the infraslow oscillation in sigma power modulates the arousal threshold during NREMs (46). During the falling phase of the infraslow oscillation, mice easily wake up in response to external stimuli, whereas they tend to sleep through during the rising phase (46, 73). The LC becomes activated during the falling phase, likely rendering this NREMs substage more fragile, as increased LC activity has been demonstrated to underlie awakenings from sleep by external stimuli (58). The increased number of calcium transients after stress likely further destabilizes sleep, reflected in the increased number of MAs and the weakened strength of the infraslow modulation. In humans, the changing levels of arousability from sleep are also reflected in different EEG/polysomnography patterns (108, 109), and people with insomnia show an increased sensitivity to wake up in response to auditory stimuli (110). Patients with PTSD also exhibit frequent arousals during sleep and suffer from reduced sleep efficiency (111, 112). Increased NE levels in the cerebrospinal fluid of PTSD patients (113) are indicative of heightened LC activity, and high plasma NE levels during sleep are negatively correlated with sleep efficiency (114). The inverse agonist for the alpha 1 adrenergic receptor prazosin is known to improve sleep in PTSD patients (115). These results further support a crucial role of NE in regulating arousal thresholds during sleep after stress. We speculate that the stress-induced changes in the infraslow LC dynamics during sleep may mechanistically contribute to the sleep disturbances often observed in patients with insomnia or PTSD (8, 116).

Together, our results provide important insights into the neural circuit mechanisms by which changes in the sleep-dependent activity of LC neurons and their projections to the POA impair sleep quality. Understanding the molecular mechanisms underlying the altered dynamics of LC neurons after stress may provide targets for pharmaceutical interventions to cure stress-related psychiatric disorders.

Materials and Methods

The *SI Appendix* includes detailed methods. DBH-Cre mice and TH-Cre mice were used. All of the procedures were approved by Institutional Animal Care and Use Committees of the University of Pennsylvania and were done in accordance with the federal regulations and guidelines on animal experimentation (National Institutes of Health Offices of Laboratory Animal Welfare Policy). For sleep recordings, EEG and EMG signals were recorded using an RHD2132 amplifier (Intan Technologies) connected to the RHD USB Interface Board (Intan Technologies). For fiber photometry, we used a Tucker-Davis Technologies RZ5P amplifier. For optogenetic stimulation, light pulses were generated by a blue laser (473nm, Laserglow) and sent through the optic fiber (ThorLabs) that connects to the ferrule on the mouse head. At the end of the experiment, mice were deeply anesthetized and transcardially perfused with phosphate-buffered saline (PBS) followed by 4% paraformaldehyde in PBS for subsequent histology to confirm virus expression and optic fiber placement.

Data, Materials, and Software Availability. The code used for data analysis is publicly available from https://github.com/tortugar/Lab (117).

The data in this study are included as *SI Appendix*, Dataset S1.

ACKNOWLEDGMENTS. This work was supported by the National Institutes of Health National Institute of Neurological Disorders and Stroke (R01-NS-110865), the Whitehall Foundation, the Alfred P. Sloan Foundation, a NARSAD Young Investigator grant by the Brain & Behavior Research Foundation, a Simons Foundation Pilot Award, an Eagle Autism Challenge Pilot Grant, the Thomas B. and Jeannette E. Laws McCabe Fund Award, The Hartwell Individual Biomedical Research Award (to S.C.), the National Institute of Health (NIH)/National Heart, Lung, and Blood Institute (NHLBI) (R01HL149133) (to F.W.) and the Sigrid Juselius Postdoctoral Fellowship (to H.A.). We thank Angela Yang for help with sleep annotations and histology, and members from the Chung and Weber labs for helpful discussion. We thank Sigrid Veasey, Seema Bhatnagar, and David Raizen for critical comments on our study.

Author affiliations: [a]Department of Neuroscience, Chronobiology, and Sleep Institute, Perelman School of Medicine, University of Pennsylvania, Philadelphia, PA 19104; [b]Department of Anesthesiology and Critical Care Medicine, The Children's Hospital of Philadelphia Research Institute, Philadelphia, PA 19104; [c]Department of Physiology and Biophysics, School of Medicine, University of California, Irvine, CA 92617; and [d]Department of Pharmacology, Perelman School of Medicine, University of Pennsylvania, Philadelphia, PA 19104

1. P. P. Chang, D. E. Ford, L. A. Mead, L. Cooper-Patrick, M. J. Klag, Insomnia in young men and subsequent depression. The Johns Hopkins Precursors Study. *Am. J. Epidemiol.* **146**, 105–114 (1997).
2. D. E. Ford, D. B. Kamerow, Epidemiologic study of sleep disturbances and psychiatric disorders. An opportunity for prevention? *JAMA* **262**, 1479–1484 (1989).
3. D. Koren, I. Arnon, P. Lavie, E. Klein, Sleep complaints as early predictors of posttraumatic stress disorder: A 1-year prospective study of injured survivors of motor vehicle accidents. *Am. J. Psychiatry* **159**, 855–857 (2002).
4. P. Meerlo, R. Havekes, A. Steiger, Chronically restricted or disrupted sleep as a causal factor in the development of depression. *Curr. Top. Behav. Neurosci.* **25**, 459–481 (2015).
5. D. Neckelmann, A. Mykletun, A. A. Dahl, Chronic insomnia as a risk factor for developing anxiety and depression. *Sleep* **30**, 873–880 (2007).
6. A. G. Harvey, C. Jones, D. A. Schmidt, Sleep and posttraumatic stress disorder: A review. *Clin. Psychol. Rev.* **23**, 377–407 (2003).
7. E.-J. Kim, J. E. Dimsdale, The effect of psychosocial stress on sleep: A review of polysomnographic evidence. *Behav. Sleep Med.* **5**, 256–278 (2007).
8. P. Lavie, Sleep disturbances in the wake of traumatic events. *N. Engl. J. Med.* **345**, 1825–1832 (2001).
9. A. C. Pawlyk, A. R. Morrison, R. J. Ross, F. X. Brennan, Stress-induced changes in sleep in rodents: Models and mechanisms. *Neurosci. Biobehav. Rev.* **32**, 99–117 (2008).
10. L. D. Sanford, D. Suchecki, P. Meerlo, "Stress, arousal, and sleep" in *Sleep, Neuronal Plasticity and Brain Function. Current Topics in Behavioral Neurosciences*, v. **25**, P. Meerlo, R. M. Benca, T. Abel, Eds. (Springer, 2015), pp. 379–410.
11. J. G. McCoy *et al.*, Experimental sleep fragmentation impairs attentional set-shifting in rats. *Sleep* **30**, 52–60 (2007).
12. A. Rolls *et al.*, Optogenetic disruption of sleep continuity impairs memory consolidation. *Proc. Natl. Acad. Sci. U.S.A.* **108**, 13305–13310 (2011).
13. J. L. Tartar *et al.*, Experimental sleep fragmentation and sleep deprivation in rats increases exploration in an open field test of anxiety while increasing plasma corticosterone levels. *Behav. Brain Res.* **197**, 450–453 (2009).
14. Y. D. Van Der Werf *et al.*, Sleep benefits subsequent hippocampal functioning. *Nat. Neurosci.* **12**, 122–123 (2009).
15. L. Palagini, C. Baglioni, A. Ciapparelli, A. Gemignani, D. Riemann, REM sleep dysregulation in depression: State of the art. *Sleep Med. Rev.* **17**, 377–390 (2013).
16. R. J. Ross *et al.*, Rapid eye movement sleep disturbance in posttraumatic stress disorder. *Biol. Psychiatry* **35**, 195–202 (1994).
17. E. J. W. Van Someren, Brain mechanisms of insomnia: New perspectives on causes and consequences. *Physiol. Rev.* **101**, 995–1046 (2021).
18. A. Ahnaou, W. H. I. M. Drinkenburg, Simultaneous changes in sleep, qEEG, physiology, behaviour and neurochemistry in rats exposed to repeated social defeat stress. *Neuropsychobiology* **73**, 209–223 (2016).
19. X. Feng *et al.*, Anxiolytic effect of increased NREM sleep after acute social defeat stress in mice. *Neurosci. Bull.* **36**, 1137–1146 (2020).
20. S. Fujii, M. K. Kaushik, X. Zhou, M. Korkutata, M. Lazarus, Acute social defeat stress increases sleep in mice. *Front. Neurosci.* **13**, 322 (2019).
21. L. A. Grafe *et al.*, Passive coping strategies during repeated social defeat are associated with long-lasting changes in sleep in rats. *Front. Syst. Neurosci.* **14**, 6 (2020).
22. F. Henderson, V. Vialou, S. El Mestikawy, V. Fabre, Effects of social defeat stress on sleep in mice. *Front. Behav. Neurosci.* **11**, 227 (2017).
23. A. M. Kinn Rød *et al.*, Effects of social defeat on sleep and behaviour: Importance of the confrontational behaviour. *Physiol. Behav.* **127**, 54–63 (2014).
24. P. Meerlo, F. W. Turek, Effects of social stimuli on sleep in mice: Non-rapid-eye-movement (NREM) sleep is promoted by aggressive interaction but not by sexual interaction. *Brain Res.* **907**, 84–92 (2001).
25. G. G. Page, M. R. Opp, S. L. Kozachik, Sex differences in sleep, anhedonia, and HPA axis activity in a rat model of chronic social defeat. *Neurobiol. Stress* **3**, 105–113 (2016).
26. A. M. Wells *et al.*, Effects of chronic social defeat stress on sleep and circadian rhythms are mitigated by kappa-opioid receptor antagonism. *J. Neurosci.* **37**, 7656–7668 (2017).
27. G. Aston-Jones, J. D. Cohen, An integrative theory of locus coeruleus-norepinephrine function: Adaptive gain and optimal performance. *Annu. Rev. Neurosci.* **28**, 403–450 (2005).
28. C. W. Berridge, B. E. Schmeichel, R. A. España, Noradrenergic modulation of wakefulness/arousal. *Sleep Med. Rev.* **16**, 187–197 (2012).
29. D. J. Chandler *et al.*, Redefining noradrenergic neuromodulation of behavior: Impacts of a modular locus coeruleus architecture. *J. Neurosci.* **39**, 8239–8249 (2019).
30. G. R. Poe *et al.*, Locus coeruleus: A new look at the blue spot. *Nat. Rev. Neurosci.* **21**, 644–659 (2020).
31. S. J. Sara, The locus coeruleus and noradrenergic modulation of cognition. *Nat. Rev. Neurosci.* **10**, 211–223 (2009).
32. R. J. Valentino, E. Van Bockstaele, Convergent regulation of locus coeruleus activity as an adaptive response to stress. *Eur. J. Pharmacol.* **583**, 194–203 (2008).
33. G. Aston-Jones, F. E. Bloom, Norepinephrine-containing locus coeruleus neurons in behaving rats exhibit pronounced responses to non-noxious environmental stimuli. *J. Neurosci.* **1**, 887–900 (1981).
34. S. Bouret, S. J. Sara, Reward expectation, orientation of attention and locus coeruleus-medial frontal cortex interplay during learning. *Eur. J. Neurosci.* **20**, 791–802 (2004).
35. E. C. Clayton, J. Rajkowski, J. D. Cohen, G. Aston-Jones, Phasic activation of monkey locus ceruleus neurons by simple decisions in a forced-choice task. *J. Neurosci.* **24**, 9914–9920 (2004).
36. O. Eschenko, S. J. Sara, Learning-dependent, transient increase of activity in noradrenergic neurons of locus coeruleus during slow wave sleep in the rat: Brain stem-cortex interplay for memory consolidation? *Cereb. Cortex N. Y. N 1991* **18**, 2596–2603 (2008).
37. B. L. Jacobs, Single unit activity of locus coeruleus neurons in behaving animals. *Prog. Neurobiol.* **27**, 183–194 (1986).
38. J. G. McCall *et al.*, CRH engagement of the locus coeruleus noradrenergic system mediates stress-induced anxiety. *Neuron* **87**, 605–620 (2015).
39. J. Rajkowski, P. Kubiak, G. Aston-Jones, Locus coeruleus activity in monkey: Phasic and tonic changes are associated with altered vigilance. *Brain Res. Bull.* **35**, 607–616 (1994).
40. K. Rasmussen, D. A. Morilak, B. L. Jacobs, Single unit activity of locus coeruleus neurons in the freely moving cat. I. During naturalistic behaviors and in response to simple and complex stimuli. *Brain Res.* **371**, 324–334 (1986).
41. A. Vankov, A. Hervé-Minvielle, S. J. Sara, Response to novelty and its rapid habituation in locus coeruleus neurons of the freely exploring rat. *Eur. J. Neurosci.* **7**, 1180–1187 (1995).
42. G. A. Zitnik, A. L. Curtis, S. K. Wood, J. Arner, R. J. Valentino, Adolescent social stress produces an enduring activation of the rat locus coeruleus and alters its coherence with the prefrontal cortex. *Neuropsychopharmacology* **41**, 1376–1385 (2016).
43. G. Cano, T. Mochizuki, C. B. Saper, Neural circuitry of stress-induced insomnia in rats. *J. Neurosci.* **28**, 10167–10184 (2008).
44. A. Osorio-Forero *et al.*, Noradrenergic circuit control of non-REM sleep substates. *Curr. Biol.* **31**, 5009–5023.e7 (2021).
45. M. Bandarabadi *et al.*, A role for spindles in the onset of rapid eye movement sleep. *Nat. Commun.* **11**, 5247 (2020).
46. S. Lecci *et al.*, Coordinated infraslow neural and cardiac oscillations mark fragility and offline periods in mammalian sleep. *Sci. Adv.* **3**, e1602026 (2017).
47. J. A. Stucynski, A. L. Schott, J. Baik, S. Chung, F. Weber, Regulation of REM sleep by inhibitory neurons in the dorsomedial medulla. *Curr. Biol.* **32**, 37–50.e6 (2022).
48. S. Chung *et al.*, Identification of preoptic sleep neurons using retrograde labelling and gene profiling. *Nature* **545**, 477–481 (2017).
49. J. Lu, M. A. Greco, P. Shiromani, C. B. Saper, Effect of lesions of the ventrolateral preoptic nucleus on NREM and REM sleep. *J. Neurosci.* **20**, 3830–3842 (2000).
50. D. J. McGinty, M. B. Sterman, Sleep suppression after basal forebrain lesions in the cat. *Science* **160**, 1253–1255 (1968).
51. J. E. Sherin, P. J. Shiromani, R. W. McCarley, C. B. Saper, Activation of ventrolateral preoptic neurons during sleep. *Science* **271**, 216–219 (1996).

52. R. Szymusiak, N. Alam, T. L. Steininger, D. McGinty, Sleep-waking discharge patterns of ventrolateral preoptic/anterior hypothalamic neurons in rats. *Brain Res.* **803**, 178–188 (1998).
53. Z. Zhang *et al.*, Neuronal ensembles sufficient for recovery sleep and the sedative actions of α2 adrenergic agonists. *Nat. Neurosci.* **18**, 553–561 (2015).
54. C. W. Berridge, J. O'Neill, Differential sensitivity to the wake-promoting actions of norepinephrine within the medial preoptic area and the substantia innominata. *Behav. Neurosci.* **115**, 165–174 (2001).
55. Y. Liang *et al.*, The NAergic locus coeruleus-ventrolateral preoptic area neural circuit mediates rapid arousal from sleep. *Curr. Biol.* **31**, 3729–3742.e5 (2021).
56. T. Osaka, H. Matsumura, Noradrenergic inputs to sleep-related neurons in the preoptic area from the locus coeruleus and the ventrolateral medulla in the rat. *Neurosci. Res.* **19**, 39–50 (1994).
57. G. Aston-Jones, F. E. Bloom, Activity of norepinephrine-containing locus coeruleus neurons in behaving rats anticipates fluctuations in the sleep-waking cycle. *J. Neurosci.* **1**, 876–886 (1981).
58. H. Hayat *et al.*, Locus coeruleus norepinephrine activity mediates sensory-evoked awakenings from sleep. *Sci. Adv.* **6**, eaaz4232 (2020).
59. K. M. Swift *et al.*, Abnormal locus coeruleus sleep activity alters sleep signatures of memory consolidation and impairs place cell stability and spatial memory. *Curr. Biol.* **28**, 3599–3609.e4 (2018).
60. K. Takahashi, Y. Kayama, J. S. Lin, K. Sakai, Locus coeruleus neuronal activity during the sleep-waking cycle in mice. *Neuroscience* **169**, 1115–1126 (2010).
61. Z. I. Lázár, D.-J. Dijk, A. S. Lázár, Infraslow oscillations in human sleep spindle activity. *J. Neurosci. Methods* **316**, 22–34 (2019).
62. Ö. Yüzgeç, M. Prsa, R. Zimmermann, D. Huber, Pupil size coupling to cortical states protects the stability of deep sleep via parasympathetic modulation. *Curr. Biol.* **28**, 392–400.e3 (2018).
63. P. Halász, O. Kundra, P. Rajna, I. Pál, M. Vargha, Micro-arousals during nocturnal sleep. *Acta Physiol. Acad. Sci. Hung.* **54**, 1–12 (1979).
64. G. Z. Dos Santos Lima *et al.*, Hippocampal and cortical communication around micro-arousals in slow-wave sleep. *Sci. Rep.* **9**, 5876 (2019).
65. B. O. Watson, D. Levenstein, J. P. Greene, J. N. Gelinas, G. Buzsáki, Network homeostasis and state dynamics of neocortical sleep. *Neuron* **90**, 839–852 (2016).
66. L. M. J. Fernandez, A. Lüthi, Sleep spindles: Mechanisms and functions. *Physiol. Rev.* **100**, 805–868 (2020).
67. S.-H. Park *et al.*, A probabilistic model for the ultradian timing of REM sleep in mice. *PLOS Comput. Biol.* **17**, e1009316 (2021).
68. Y. Li *et al.*, Retrograde optogenetic characterization of the pontospinal module of the locus coeruleus with a canine adenoviral vector. *Brain Res.* **1641** (Pt B), 274–290 (2016).
69. C. Wissing, M. Maheu, S. Wiegert, A. Dieter, Targeting noradrenergic neurons of the locus coeruleus: A comparison of model systems and strategies. *bioRxiv* Preprint (2022). https://doi.org/10.1101/2022.01.22.477348.
70. C. M. Funk *et al.*, Role of somatostatin-positive cortical interneurons in the generation of sleep slow waves. *J. Neurosci.* **37**, 9132–9148 (2017).
71. J. Traut, *et al.*, Effects of clozapine-N-oxide and compound 21 on sleep in laboratory mice. *bioRxiv* Preprint (2022). https://doi.org/10.1101/2022.02.01.478652.
72. C. Varin, P.-H. Luppi, P. Fort, Melanin-concentrating hormone-expressing neurons adjust slow-wave sleep dynamics to catalyze paradoxical (REM) sleep. *Sleep (Basel)* **41**, zsy068 (2018).
73. R. Cardis *et al.*, Cortico-autonomic local arousals and heightened somatosensory arousability during NREMS of mice in neuropathic pain. *eLife* **10**, e65835 (2021).
74. T. Gallopin *et al.*, Identification of sleep-promoting neurons in vitro. *Nature* **404**, 992–995 (2000).
75. T. Gallopin *et al.*, The endogenous somnogen adenosine excites a subset of sleep-promoting neurons via A2A receptors in the ventrolateral preoptic nucleus. *Neuroscience* **134**, 1377–1390 (2005).
76. J. Feng *et al.*, A genetically encoded fluorescent sensor for rapid and specific in vivo detection of norepinephrine. *Neuron* **102**, 745–761.e8 (2019).
77. K. T. Beier *et al.*, Circuit architecture of VTA dopamine neurons revealed by systematic input-output mapping. *Cell* **162**, 622–634 (2015).
78. L. A. Schwarz *et al.*, Viral-genetic tracing of the input-output organization of a central noradrenaline circuit. *Nature* **524**, 88–92 (2015).
79. F. Weber *et al.*, Control of REM sleep by ventral medulla GABAergic neurons. *Nature* **526**, 435–438 (2015).
80. K. Takahashi, J.-S. Lin, K. Sakai, Characterization and mapping of sleep-waking specific neurons in the basal forebrain and preoptic hypothalamus in mice. *Neuroscience* **161**, 269–292 (2009).
81. O. Eschenko, C. Magri, S. Panzeri, S. J. Sara, Noradrenergic neurons of the locus coeruleus are phase locked to cortical up-down states during sleep. *Cereb. Cortex* **22**, 426–435 (2012).
82. C. Kjaerby, *et al.*, Dynamic fluctuations of the locus coeruleus-norepinephrine system underlie sleep state transitions. *Nat. Neurosci.* **25**, 1059–1070 (2022).
83. F. Weber *et al.*, Regulation of REM and non-REM sleep by periaqueductal GABAergic neurons. *Nat. Commun.* **9**, 354 (2018).
84. P. Franken, A. Malafosse, M. Tafti, Genetic determinants of sleep regulation in inbred mice. *Sleep* **22**, 155–169 (1999).
85. C.-C. Lo *et al.*, Common scale-invariant patterns of sleep-wake transitions across mammalian species. *Proc. Natl. Acad. Sci. U.S.A.* **101**, 17545–17548 (2004).
86. I. Tobler *et al.*, Altered circadian activity rhythms and sleep in mice devoid of prion protein. *Nature* **380**, 639–642 (1996).
87. M. E. Carter *et al.*, Tuning arousal with optogenetic modulation of locus coeruleus neurons. *Nat. Neurosci.* **13**, 1526–1533 (2010).
88. H. S. Gompf, E. A. Budygin, P. M. Fuller, C. E. Bass, Targeted genetic manipulations of neuronal subtypes using promoter-specific combinatorial AAVs in wild-type animals. *Front. Behav. Neurosci.* **9**, 152 (2015).
89. K. A. Porter-Stransky *et al.*, Noradrenergic transmission at alpha1-adrenergic receptors in the ventral periaqueductal gray modulates arousal. *Biol. Psychiatry* **85**, 237–247 (2019).
90. S. Lammel *et al.*, Diversity of transgenic mouse models for selective targeting of midbrain dopamine neurons. *Neuron* **85**, 429–438 (2015).
91. J. Lindeberg *et al.*, Transgenic expression of Cre recombinase from the tyrosine hydroxylase locus. Genesis **40**, 67–73 (2004).
92. N. Min, T. H. Joh, K. S. Kim, C. Peng, J. H. Son, 5′ upstream DNA sequence of the rat tyrosine hydroxylase gene directs high-level and tissue-specific expression to catecholaminergic neurons in the central nervous system of transgenic mice. *Brain Res. Mol. Brain Res.* **27**, 281–289 (1994).
93. J. M. Savitt, S. S. Jang, W. Mu, V. L. Dawson, T. M. Dawson, Bcl-x is required for proper development of the mouse substantia nigra. *J. Neurosci.* **25**, 6721–6728 (2005).
94. J. R. Cho *et al.*, Dorsal Raphe dopamine neurons modulate arousal and promote wakefulness by salient stimuli. *Neuron* **94**, 1205–1219.e8 (2017).
95. M. H. Qiu, M. C. Chen, P. M. Fuller, J. Lu, Stimulation of the pontine parabrachial nucleus promotes wakefulness via extra-thalamic forebrain circuit nodes. *Curr. Biol.* **26**, 2301–2312 (2016).
96. Q. Xu *et al.*, Medial parabrachial nucleus is essential in controlling wakefulness in rats. *Front. Neurosci.* **15**, 645877 (2021).
97. C. Blanco-Centurion, D. Gerashchenko, P. J. Shiromani, Effects of saporin-induced lesions of three arousal populations on daily levels of sleep and wake. *J. Neurosci.* **27**, 14041–14048 (2007).
98. M. S. Hunsley, R. D. Palmiter, Norepinephrine-deficient mice exhibit normal sleep-wake states but have shorter sleep latency after mild stress and low doses of amphetamine. *Sleep* **26**, 521–526 (2003).
99. B. E. Jones, S. T. Harper, A. E. Halaris, Effects of locus coeruleus lesions upon cerebral monoamine content, sleep-wakefulness states and the response to amphetamine in the cat. *Brain Res.* **124**, 473–496 (1977).
100. P. Lidbrink, The effect of lesions of ascending noradrenaline pathways on sleep and waking in the rat. *Brain Res.* **74**, 19–40 (1974).
101. P. Delagrange, M. H. Canu, A. Rougeul, P. Buser, J. J. Bouyer, Effects of locus coeruleus lesions on vigilance and attentive behaviour in cat. *Behav. Brain Res.* **53**, 155–165 (1993).
102. J. M. Monti, L. D'Angelo, H. Jantos, L. Barbeito, V. Abó, Effect of DSP-4, a noradrenergic neurotoxin, on sleep and wakefulness and sensitivity to drugs acting on adrenergic receptors in the rat. *Sleep* **11**, 370–377 (1988).
103. M. Ouyang, K. Hellman, T. Abel, S. A. Thomas, Adrenergic signaling plays a critical role in the maintenance of waking and in the regulation of REM sleep. *J. Neurophysiol.* **92**, 2071–2082 (2004).
104. H. Yamaguchi, F. W. Hopf, S.-B. Li, L. de Lecea, In vivo cell type-specific CRISPR knockdown of dopamine beta hydroxylase reduces locus coeruleus evoked wakefulness. *Nat. Commun.* **9**, 5211 (2018).
105. I. Gvilia, A. Turner, D. McGinty, R. Szymusiak, Preoptic area neurons and the homeostatic regulation of rapid eye movement sleep. *J. Neurosci.* **26**, 3037–3044 (2006).
106. J. Lu *et al.*, Selective activation of the extended ventrolateral preoptic nucleus during rapid eye movement sleep. *J. Neurosci.* **22**, 4568–4576 (2002).
107. G.-W. Zhang *et al.*, Medial preoptic area antagonistically mediates stress-induced anxiety and parental behavior. *Nat. Neurosci.* **24**, 516–528 (2021).
108. M. G. Terzano *et al.*, The cyclic alternating pattern as a physiologic component of normal NREM sleep. *Sleep* **8**, 137–145 (1985).
109. M. G. Terzano *et al.*, CAP variables and arousals as sleep electroencephalogram markers for primary insomnia. *Clin. Neurophysiol.* **114**, 1715–1723 (2003).
110. B. Feige *et al.*, The microstructure of sleep in primary insomnia: An overview and extension. *Int. J. Psychophysiol.* **89**, 171–180 (2013).
111. A. Germain, Sleep disturbances as the hallmark of PTSD: Where are we now? *Am. J. Psychiatry* **170**, 372–382 (2013).
112. A. Germain, D. J. Buysse, E. Nofzinger, Sleep-specific mechanisms underlying posttraumatic stress disorder: Integrative review and neurobiological hypotheses. *Sleep Med. Rev.* **12**, 185–195 (2008).
113. T. D. Geracioti, Jr *et al.*, CSF norepinephrine concentrations in posttraumatic stress disorder. *Am. J. Psychiatry* **158**, 1227–1230 (2001).
114. T. A. Mellman, A. Kumar, R. Kulick-Bell, M. Kumar, B. Nolan, Nocturnal/daytime urine noradrenergic measures and sleep in combat-related PTSD. *Biol. Psychiatry* **38**, 174–179 (1995).
115. F. Taylor, M. A. Raskind, The alpha1-adrenergic antagonist prazosin improves sleep and nightmares in civilian trauma posttraumatic stress disorder. *J. Clin. Psychopharmacol.* **22**, 82–85 (2002).
116. P. Halász, M. Terzano, L. Parrino, R. Bódizs, The nature of arousal in sleep. *J. Sleep Res.* **13**, 1–23 (2004).
117. https://github.com/tortugar/Lab. GitHub. Deposited 22 September 2022.